

27

NAVAL POSTGRADUATE SCHOOL Monterey, California

AD-A164 355



DTIC
ELECTE
FEB 20 1986
S D
D

THESIS

A COMPARISON OF TWO METHODS FOR FIBER
DIAMETER MEASUREMENT AND A SYSTEM DESIGN
FOR THE STUDY OF COMPOSITE RELIABILITY

by

Thomas Alvin Bennett

December 1985

Thesis Advisor:

Edward M. Wu

DATA FILE COPY

Approved for public release,
distribution is unlimited

86 2 20 031

REPORT DOCUMENTATION PAGE

1a. REPORT SECURITY CLASSIFICATION		1b. RESTRICTIVE MARKINGS	
2a. SECURITY CLASSIFICATION AUTHORITY		3. DISTRIBUTION/AVAILABILITY OF REPORT Approved for public release, distribution is unlimited	
2b. DECLASSIFICATION/DOWNGRADING SCHEDULE			
4. PERFORMING ORGANIZATION REPORT NUMBER(S)		5. MONITORING ORGANIZATION REPORT NUMBER(S)	
6a. NAME OF PERFORMING ORGANIZATION Naval Postgraduate School	6b. OFFICE SYMBOL (if applicable) Code 67	7a. NAME OF MONITORING ORGANIZATION Naval Postgraduate School	
6c. ADDRESS (City, State, and ZIP Code) Monterey, California 93943-5100		7b. ADDRESS (City, State, and ZIP Code) Monterey, California 93943-5100	
8a. NAME OF FUNDING/SPONSORING ORGANIZATION	8b. OFFICE SYMBOL (if applicable)	9. PROCUREMENT INSTRUMENT IDENTIFICATION NUMBER	
8c. ADDRESS (City, State, and ZIP Code)		10. SOURCE OF FUNDING NUMBERS	
		PROGRAM ELEMENT NO	PROJECT NO
		TASK NO	WORK UNIT ACCESSION NO
11. TITLE (Include Security Classification) A COMPARISON OF TWO METHODS FOR FIBER DIAMETER MEASUREMENT AND A SYSTEM DESIGN FOR THE STUDY OF COMPOSITE RELIABILITY			
12. PERSONAL AUTHOR(S) Bennett, Thomas A.			
13a. TYPE OF REPORT Master's Thesis	13b. TIME COVERED FROM _____ TO _____	14. DATE OF REPORT (Year, Month, Day) 1985 December	15. PAGE COUNT 73
16. SUPPLEMENTARY NOTATION			
17. COSATI CODES		18. SUBJECT TERMS (Continue on reverse if necessary and identify by block number)	
FIELD	GROUP	SUB-GROUP	
		Methods of fiber diameter measurement using laser diffraction pattern, integrated systems	
19. ABSTRACT (Continue on reverse if necessary and identify by block number) This thesis involves the design and construction of an integrated fiber diameter measurement and strength test system for the purpose of conducting a study of the reliability of a composite material. The emphasis of this thesis is placed on the comparison of two methods of fiber diameter measurement using the light diffraction pattern formed by the obstruction of a laser beam by a fiber sample. K... ..			
20. DISTRIBUTION/AVAILABILITY OF ABSTRACT <input checked="" type="checkbox"/> UNCLASSIFIED/UNLIMITED <input type="checkbox"/> SAME AS RPT <input type="checkbox"/> DTIC USERS		21. ABSTRACT SECURITY CLASSIFICATION unclassified	
22a. NAME OF RESPONSIBLE INDIVIDUAL Edward M. Wu		22b. TELEPHONE (Include Area Code) 646-3459	22c. OFFICE SYMBOL 67-wt

Approved for public release, distribution is unlimited

**A Comparison of Two Methods for Fiber Diameter Measurement
and a System Design for the Study of Composite Reliability**

by

**Thomas Alvin Bennett
Lieutenant, United States Navy
B.S., United States Naval Academy, 1978**

**Submitted in partial fulfillment of the
requirements for the degree of**

MASTER OF SCIENCE IN ENGINEERING SCIENCE

from the

**NAVAL POSTGRADUATE SCHOOL
December 1985**

Author: *Thomas Alvin Bennett*
Thomas Alvin Bennett

Approved by: *Edward M. Wu*
Edward M. Wu, Thesis Advisor

M. F. Platzter
M.F. Platzter, Chairman, Department
of Aeronautics

John N. Dyer
John N. Dyer, Dean of Science
and Engineering

ABSTRACT

This thesis involves the design and construction of an integrated fiber diameter measurement and strength test system for the purpose of conducting a study of the reliability of a composite material. The emphasis of this thesis is placed on the comparison of two methods of fiber diameter measurement using the light diffraction pattern formed by the obstruction of a laser beam by a fiber sample.

Accession For	
NTIS CRA&I	<input checked="" type="checkbox"/>
DTIC TAB	<input type="checkbox"/>
Unannounced	<input type="checkbox"/>
Justification	
By	
Distribution /	
Availability Codes	
Dist	Avail and/or Special
A-1	

TABLE OF CONTENTS

	PAGE
I. INTRODUCTION -----	11
II. BACKGROUND -----	13
III. METHODS OF FIBER DIAMETER MEASUREMENT -----	18
A. PHOTOCONDUCTIVE CELL -----	18
1. Operation -----	21
B. MICRONEYE -----	22
1. Operation -----	24
IV. INTEGRATED FIBER DIAMETER AND STRENGTH TEST -----	30
A. SYSTEM DESCRIPTION -----	30
B. DESIGN -----	30
V. DATA COLLECTION -----	41
A. PHOTOCONDUCTIVE CELL -----	41
1. Procedure -----	41
2. Data -----	42
B. MICRONEYE -----	45
1. Procedure -----	45
2. Data -----	48
VI. STATISTICAL ANALYSIS -----	50
VII. DISCUSSION OF RESULTS -----	53
VIII. CONCLUSIONS AND RECOMMENDATIONS -----	61
APPENDIX A. SMALL ANGLE APPROXIMATION -----	63
APPENDIX B. ERROR ANALYSIS -----	65

LIST OF REFERENCES -----	70
BIBLIOGRAPHY -----	71
INITIAL DISTRIBUTION LIST -----	72

LIST OF TABLES

TABLE	PAGE
I. MEASUREMENT DATA AND CALCULATED FIBER DIAMETERS FOR METHOD A AT 0 DEGREES -----	43
II. MEASUREMENT DATA AND CALCULATED FIBER DIAMETERS FOR METHOD A AT 90 DEGREES -----	44
III. MEASUREMENT DATA AND CALCULATED FIBER DIAMETERS FOR METHOD B AT 0 AND 90 DEGREES -----	49
IV. MEAN AND STANDARD DEVIATION FOR THE FIBER DIAMETERS OF METHOD A AND B -----	52
V. DIMENSIONAL DATA FOR METHOD A AT 0 AND 90 DEGREE ASPECTS -----	65
VI. UNCERTAINTIES FOR CALCULATIONS OF METHOD A AT 0 AND 90 DEGREE ASPECTS -----	67
VII. DIMENSIONAL DATA FOR METHOD B AT 0 AND 90 DEGREE ASPECTS -----	67
VIII. UNCERTAINTIES FOR CALCULATIONS OF METHOD B AT 0 AND 90 DEGREE ASPECTS -----	68
IX. STANDARD ERROR AND STANDARD DEVIATION FOR METHODS A AND B AT 0 AND 90 DEGREE ASPECTS -----	69
X. MEAN DIAMETERS WITH PROPAGATION AND STANDARD ERROR FOR METHODS A AND B AT 0 AND 90 DEGREE ASPECTS -----	69

LIST OF REFERENCES -----	70
BIBLIOGRAPHY -----	71
INITIAL DISTRIBUTION LIST -----	72

LIST OF TABLES

TABLE	PAGE
I. MEASUREMENT DATA AND CALCULATED FIBER DIAMETERS FOR METHOD A AT 0 DEGREES -----	43
II. MEASUREMENT DATA AND CALCULATED FIBER DIAMETERS FOR METHOD A AT 90 DEGREES -----	44
III. MEASUREMENT DATA AND CALCULATED FIBER DIAMETERS FOR METHOD B AT 0 AND 90 DEGREES -----	49
IV. MEAN AND STANDARD DEVIATION FOR THE FIBER DIAMETERS OF METHOD A AND B -----	52
V. DIMENSIONAL DATA FOR METHOD A AT 0 AND 90 DEGREE ASPECTS -----	65
VI. UNCERTAINTIES FOR CALCULATIONS OF METHOD A AT 0 AND 90 DEGREE ASPECTS -----	67
VII. DIMENSIONAL DATA FOR METHOD B AT 0 AND 90 DEGREE ASPECTS -----	67
VIII. UNCERTAINTIES FOR CALCULATIONS OF METHOD B AT 0 AND 90 DEGREE ASPECTS -----	68
IX. STANDARD ERROR AND STANDARD DEVIATION FOR METHODS A AND B AT 0 AND 90 DEGREE ASPECTS -----	69
X. MEAN DIAMETERS WITH PROPAGATION AND STANDARD ERROR FOR METHODS A AND B AT 0 AND 90 DEGREE ASPECTS -----	69

LIST OF FIGURES

FIGURE		PAGE
1.	Diffraction pattern-----	14
2.	Single Slit Experiment-----	15
3.	Wavepath Difference of a Fiber Obstruction -----	16
4.	Low Power Laser and Sample Fiber-----	19
5.	Photoconductive Cells and Multimeters-----	19
6.	Parrallel Light Simulation-----	20
7.	OpticRAM Capacitor Logic-----	23
8.	OpticRAM Interleaved Pattern-----	25
9.	Mapping Circuit Logic-----	26
10.	Cell Placement Grid-----	27
11.	MicronEye Experimental Set-up-----	28
12.	MicronEye and Computer Interface-----	28
13.	Integrated System Schematic -----	31
14.	Fiber Strength Test Frame-----	33
15.	Integrated System-----	35
16.	Integrated System-----	36
17.	Integrated System-----	37
18.	Integrated System-----	38
19.	Integrated System-----	39
20.	Integrated System-----	40
21.	MicronEye Diffraction Pattern Distance-----	46

22.	MicronEye Graphics Output Pattern-----	47
23.	Photocell Method 0 Degree Aspect-----	54
24.	Photocell Method 90 Degree Aspect-----	55
25.	MicronEye Method 0 Degree Aspect-----	56
26.	MicronEye Method 90 Degree Aspect-----	57

LIST OF SYMBOLS

- a Fiber diameter
- d Distance from diffraction pattern center to integer number of nodes
- C Calibrated distance of minimum photo cell separation
- δC Change in calibrated distance
- λ Wavelength of the He-Ne laser
- θ Diffraction angle
- n integer number of wavelengths
- μ Microns
- L Distance from fiber sample to the plane of the diffraction pattern
- X Distance from node to node of opposite sides of the diffraction pattern for equal values of n
- P Number of pixels between adjacent nodes of a diffraction pattern
- k Units conversion constant
- F Distance between nodes of a diffraction pattern in microns
- v Variation
- \bar{X} Mean value of X
- σ_s Standard deviation
- σ_m Standard error
- E_s Summation error
- E_p Product error
- E_q Quotient error

ACKNOWLEDGEMENT

I am gratefully thankful to my thesis advisor Dr. Edward M. Wu for his help and contribution to this thesis. Without his ideas and encouragement this study would not have been possible. Because of Dr. Wu, I learned a great deal about composite materials, a subject I had virtually no knowledge of prior to commencement of this study. Additionally I am thankful for his generous availability of funds, equipment, computers, and facilities.

Special thanks are also given to:

Dr. Shi-Hau Own, for all his help in purchasing procedures, literature assistance, and computer software,

Ted Dunton and Bob Besel, for their technical assistance and coordination,

Glen Middleton, for his beautiful machining work in the shop.

I. INTRODUCTION

The use of composite materials in today's modern technological world is becoming increasingly popular due to the strength that composite materials have demonstrated to possess. Because of the increased manufacture and use of composites, it is important to be able to determine the strength and ultimately the reliability that a composite will have in order to better utilize its characteristics for the requirements desired. Typical composite materials consist of high strength/modulus fibers bonded with a matrix material. Reliability in a composite can be predicted based on the probability that a composite will not fail. Of the many models of failure that have been studied, the simplest is that which assumes a uniform strain existing throughout the composite material, and that fracture occurs at the failure strain of the fibers alone [Ref. 1]. In his paper, Rosen states that composite failure occurs due to uniaxial stress when the remaining unbroken fibers at the weakest cross-section are unable to resist the applied load [Ref. 1]. Composite failure therefore results from tensile fracture of the fibers. Stress is determined as a function of the applied load and the cross sectional area of the fiber. In the analysis of composite reliability, fiber diameter is necessary in determining the cross-sectional area of the fiber. This would appear not to be that difficult of a task provided the assumption is made that all fibers have the same diameter. This however is not a valid assumption since fiber diameters vary throughout

a composite as well as individually. In fact the diameter varies along the length of the fiber and the cross sectional area is not uniform [Ref.2]. Most fiber diameters being in the micron range of dimension, are difficult to resolve using conventional physical means which is why microscopic techniques are commonly used.

This thesis discusses an integrated system of equipment and instruments designed to collect data on fiber sample strength and diameter in order to provide the information necessary to perform a study on the reliability of a fiber and therefore a composite material. Although the design is ultimately intended to provide fracture load data to determine the strength of a sample fiber, the emphasis of this study is a comparison of two methods of fiber diameter measurement with demonstrated repeatability in each and the potential for computer automated measurements. In addition it will be shown that the fiber does vary in diameter.

II. BACKGROUND

The classical light diffraction experiment using a single slit obstruction is used to determine the dimension of a very small slit. This same experiment can be used as a basis to find the diameter of a very small fiber since the concept is the same in principle. Huygen's theory of light assumes that light is a wave rather than a stream of particles [Ref.3]. "Huygens' principle states that each point in a wave front acts as a source of new waves." [Ref.4] The single slit diffraction pattern can be analyzed by replacing the slit opening with a large number of obstructions and calculating the resulting diffraction pattern on a screen [Ref.5]. In this case the obstruction of light causing the diffraction pattern is a fiber sample whose diameter is the surface width of the obstruction. Diffraction is actually a kind of interference. Waves from one edge of the obstruction interfere with waves from the other edge to produce the diffraction pattern as indicated by the dark and light intensity bands in Figure 1. In the single slit experiment as seen by Figure 2, a is the width of the obstruction. The path difference from the top and bottom of the obstruction is $a \sin \theta$. If the path difference is a whole multiple of one wavelength, the first and last waves will differ in phase by 360 degrees and the resulting amplitude of the intensity due to superposition will be zero. The location of the first minima (node) in the diffraction pattern is $a \sin \theta = n \lambda$ [Ref.5]. Replacing the obstruction with the fiber sample the wave path difference due to the thickness (diameter) of the fiber is one wavelength (see Figure 3).

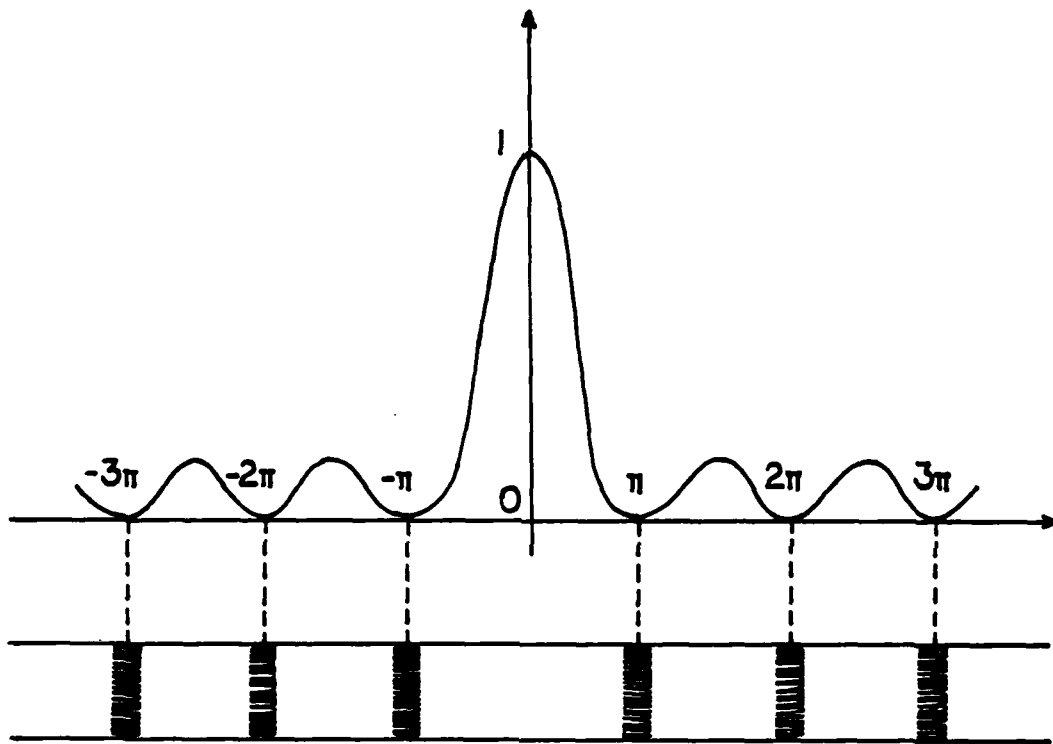


Figure 1. Diffraction Pattern

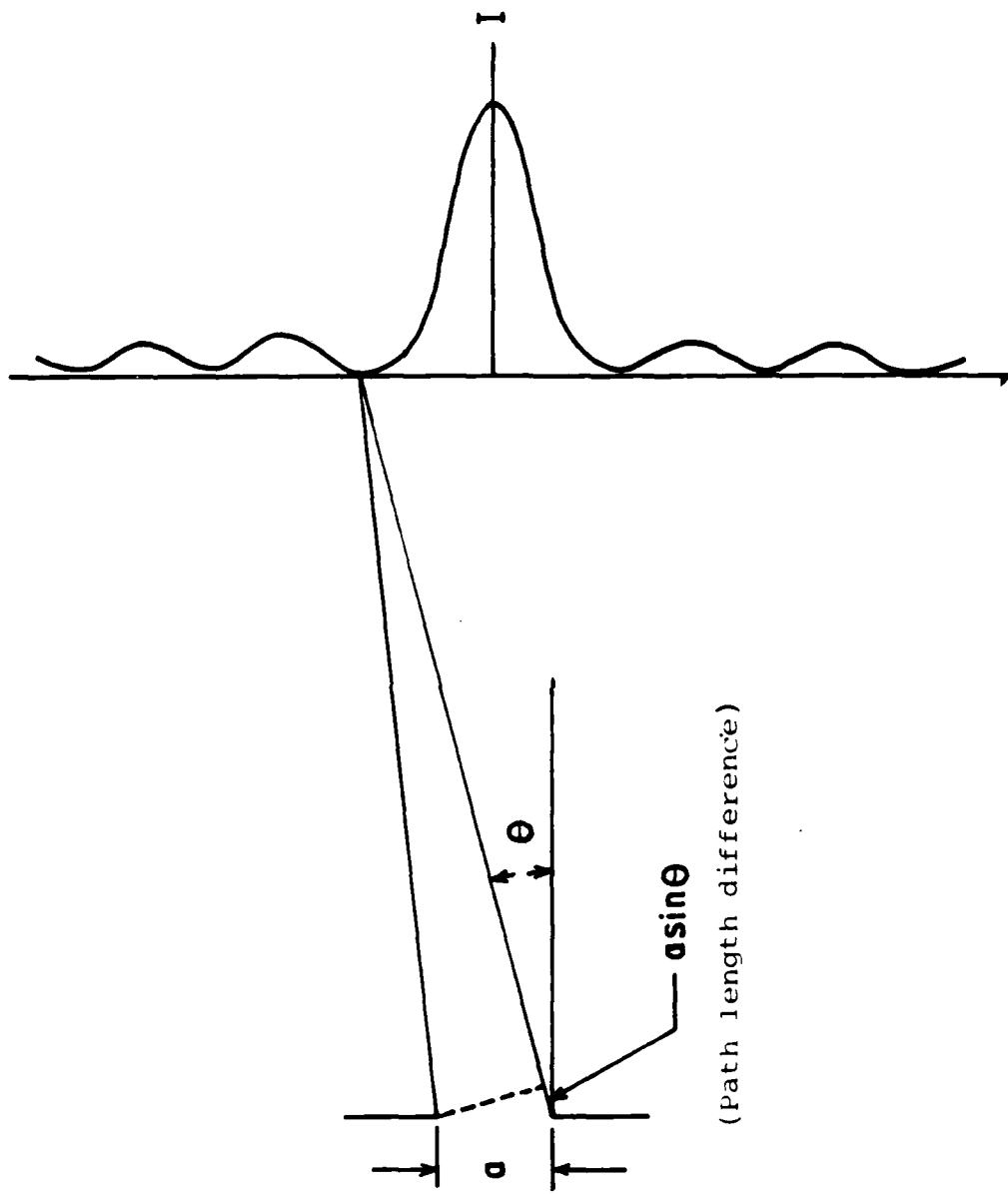


Figure 2. Single Slit Experiment

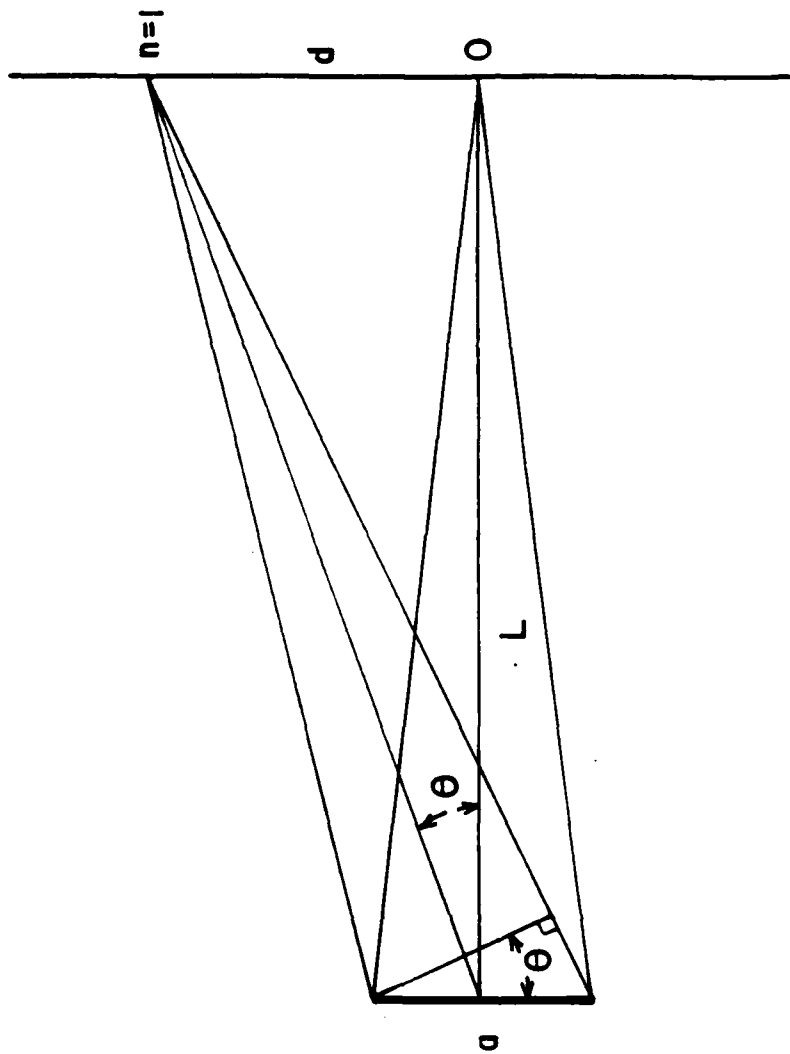


Figure 3. Wavepath Difference of a Fiber Obstruction

$$a \sin \theta = n \lambda \quad (1)$$

The single slit experiment assumes that the wavefronts arriving at the diffraction source are plane waves and that the light rays associated with these wavefronts are parallel to each other [Ref.6]. In reality wavefronts are parallel only at very large distances from the light source, called the Fraunhofer region. However, using a laser beam as the source of light together with a collimating lens, the light waves can be made parallel and therefore the Fraunhofer region can be simulated. [Ref.7] From Figure 2 it is observed that the angle theta (θ) equals the ARCTANGENT of the distance to the first node divided by the distance from the diffraction source to the diffraction pattern ($\theta = \text{ARCTAN } d/L$). Since L is much larger than d, the angle θ is very small. Using the small angle approximation, $\sin \theta \sim d/L$ (for $\theta \ll 1$), equation (1) can be simplified. Solving for the diameter of the fiber;

$$a = (L/d) n \lambda \quad (2)$$

Based on the known theory of light and the small angle approximation the diameter of a fiber can be determined.

III. METHODS OF FIBER DIAMETER MEASUREMENT

The two methods of fiber diameter measurement used in this thesis are described as follows.

A. PHOTOCONDUCTIVE CELL

This particular method of measuring the nodes of diffraction caused by the diameter of the fiber, is by light sensitive photoconductive cells. The cells are used to locate the lowest intensity of light or interference node of the particular diffraction pattern by traversing the cells perpendicular to the light source and parallel to the projected diffraction pattern. The equipment set-up is shown in Figures 4 & 5, which consists of the following: a low power Helium-Neon laser (0.52mW) with a known wavelength of light ($\lambda = 632.8 \times 10^{-9}$ meters), a spatial filter and collimating lens, two light sensitive photoconductive cells mounted in vertical pins affixed to micrometer drive positioning tables, two multimeters to read the resistance proportional to the intensity factor of the diffraction nodes, and finally a fiber sample mounted and capable of being rotated to obtain diameter data at aspect angles of 0 and 90 degrees. A spatial filter is used to nearly simulate the Fraunhofer region of light. To do this the light from the laser was passed through a very small circular hole positioned at the focal point downstream from a focussing lens. At the focal point, ideally all stray light or optical noise is effectively blocked out except for that light which passes through the aperture (See Figure 6).

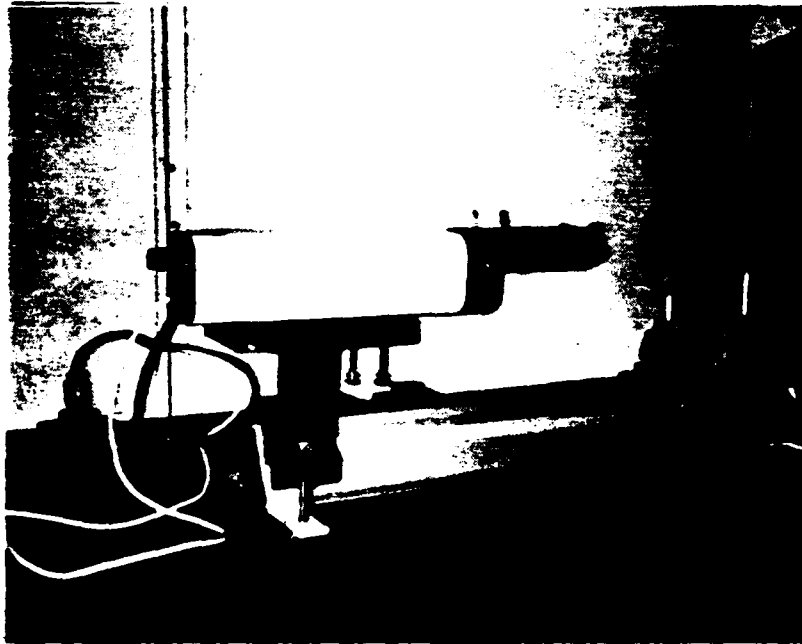


Figure 4. Low Power Laser and Sample Fiber

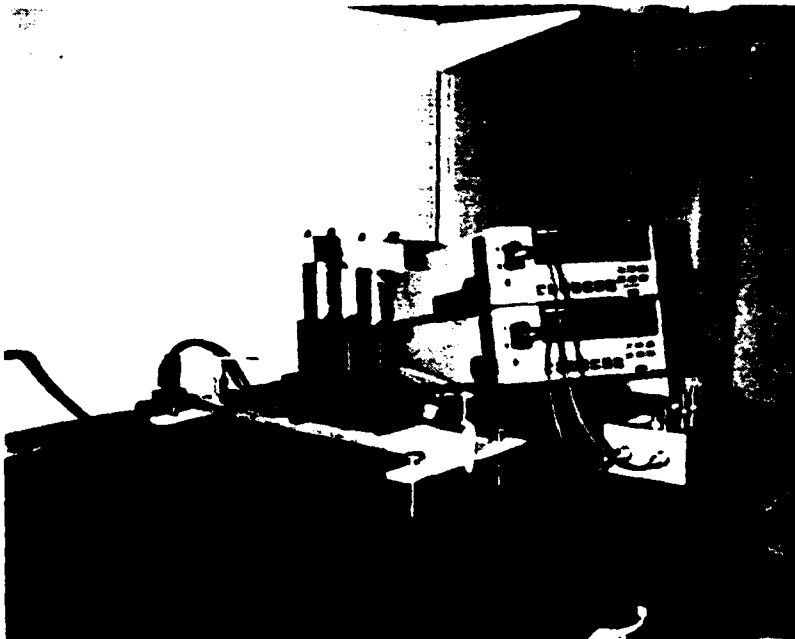


Figure 5. Photoconductive Cells and Multimeters

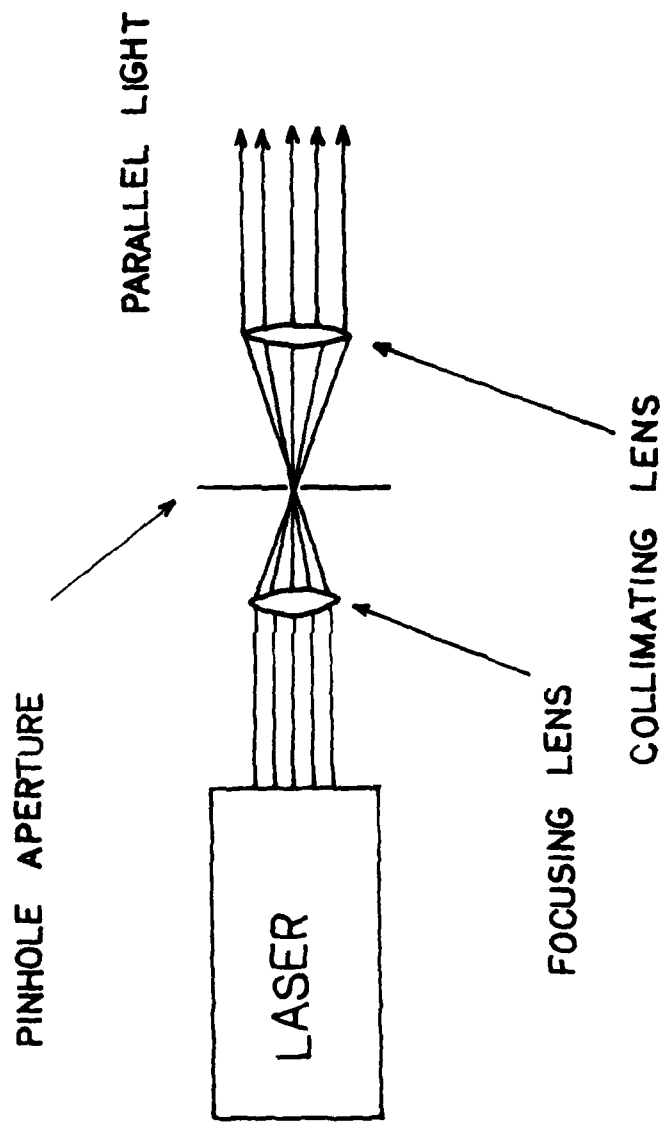


Figure 6. Parallel Light Simulation

After the light passes through the aperture it is again passed through another lens called the collimating lens placed downstream from the aperture. The light that passes through the collimating lens is essentially parallel and nearly simulates the Fraunhofer region. The entire spatial filter and collimating lens is affixed to the output port of the He-Ne Laser.

1. Operation

The operation of this set-up involves positioning the sample fiber in the path of the collimated laser light beam producing a diffraction pattern a distance L away. The further the projection of the diffraction pattern from the fiber sample, the more widespread the projected pattern. In other words the distance X between integer number of nodes is proportional to the distance between the diffraction pattern and the light obstruction. Using the photoconductive cells as sensors for high and low intensity, they are positioned parallel to the diffraction pattern. Electrical resistances are measured by the multimeter connected to the photoconductive cell. The cells are manually adjusted so as to maximize the resistance which corresponds to the center of the node in the diffraction pattern. Once the nodes on either side of the diffraction pattern are located, the distance X between the two photoconductive cells is measured using a digital micrometer caliper with resolution to 0.01 millimeters. As seen in Figure 3, the measured distance X is twice the distance d . The operation of this measurement technique is manual and dependent upon the operator's judgement for the determination of the maximum resistance readings.

B. MICRONEYE

This particular method of measurement utilizes the MicronEye which is an electro-optical system used as a peripheral for a microcomputer. The MicronEye is an OpticRAM (IS32A) developed by Micron Technology, Inc. The OpticRAM consists of 65,536 individual image sensing elements called pixels. These sensing elements made of silicon material are arranged on the IS32A microchip in two arrays consisting of 128×256 pixels each.[Ref.8]

The theory of operation for the MicronEye is as follows: An optical image is focussed on the OpticRAM which is then digitized by the sensing elements. The MicronEye (circuit card interface) transmits the digital image from the OpticRAM to the computer. A software program takes the transmitted image and displays it on a graphics screen. Because the OpticRAM is digital, the image is black and white. Each pixel on the OpticRAM is a 6.4 micron square light sensitive capacitor. Light striking a pixel will cause the capacitor, which is initially precharged to +5 volts, to discharge toward 0 volts. Discharge occurs at a rate proportional to both the intensity and duration the element is exposed to light. The OpticRAM performs a digital comparison after a specified elapsed time between the voltage still existent on the capacitor and the fixed threshold of +2.5 volts. The output pin to each pixel is set to a logic level 1 (black) if the voltage is greater than the threshold or a logic level 0 (white) if the existent voltage is less than the threshold (see Figure 7). A white pixel on the graphics screen indicates a capacitive element that was not exposed to a light intensity sufficient to discharge below the threshold point.[Ref.9] In this particular application the threshold can be changed by adjusting the exposure time or

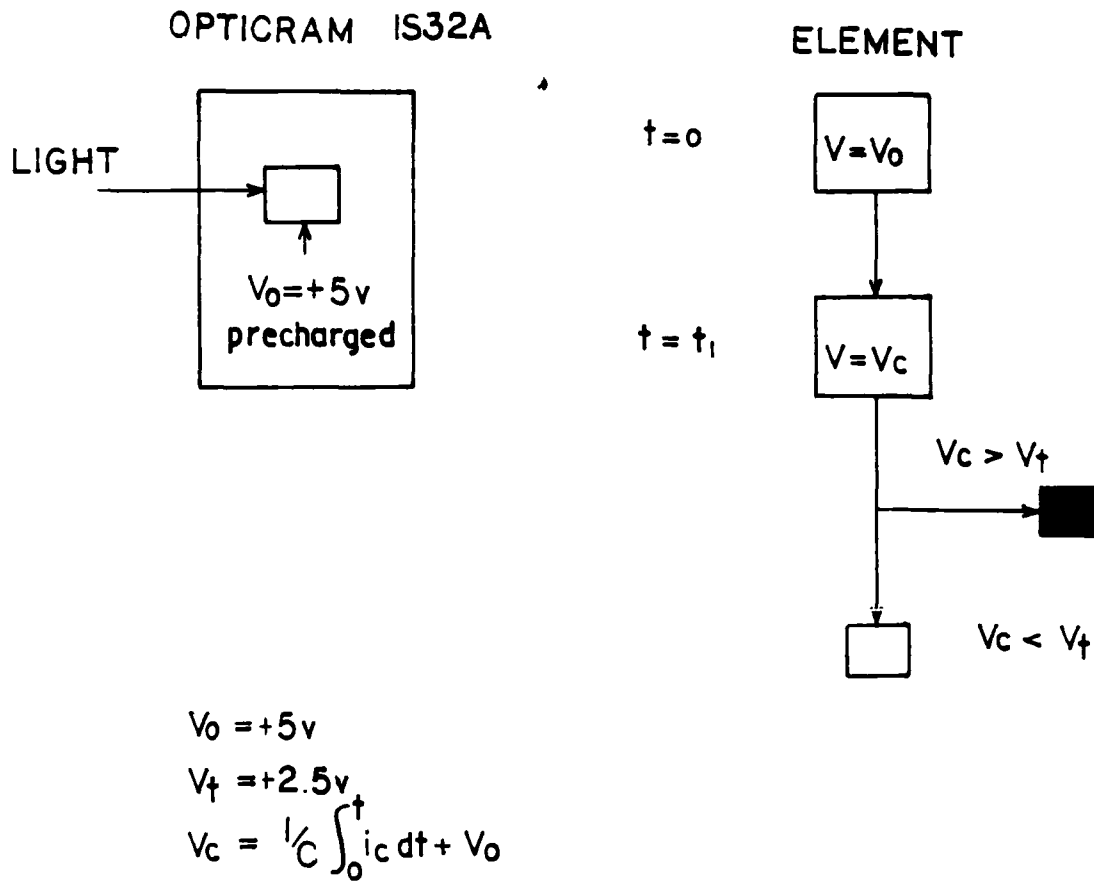


Figure 7. OpticRAM Capacitor Logic

in other words the elapsed time at which threshold comparisons are made. Increasing the exposure time causes more of an image to fall on the white side of the threshold. A REFRESH mode within the MicronEye circuitry allows each cell to be refreshed every 6.3 milliseconds. Those cells that were originally black after a specific discharge time are refreshed back to +5 volts, whereas those that discharged below the threshold after time t_1 are refreshed to 0 volts (see Figure 7). The image output from the computer can be graphically viewed on the screen or output on a graphics printer. The MicronEye is programmed to output the image on an Epson printer using a parallel interface. The output is software controlled via control codes from the computer to the printer in bit image format.

The physical arrangement of the OpticRAM IS32A is actually a staggered interleaved pattern as seen in Figure 8. In order to perform the desired mapping to graphics that corresponds one to one with the physical layout of the IS32A chip, a logic circuit depicted in Figure 9, maps the actual pixel arrangement to the topology diagram in Figure 10, called the Cell Placement Grid. In the physical layout each cell is 8.6 microns horizontal by 6.8 microns vertical in dimension. The change in dimension from the 6.4 microns square sensing element is an adjustment to account for the interleaved pattern that is compensated for during the mapping logic from physical geometry to topological arrangement.[Ref.10]

1. Operation

The equipment set-up for this method of measurement seen in Figures 11 & 12, consists of the low power He-Ne laser and fiber sample identical to method A but with the MicronEye substituted for the

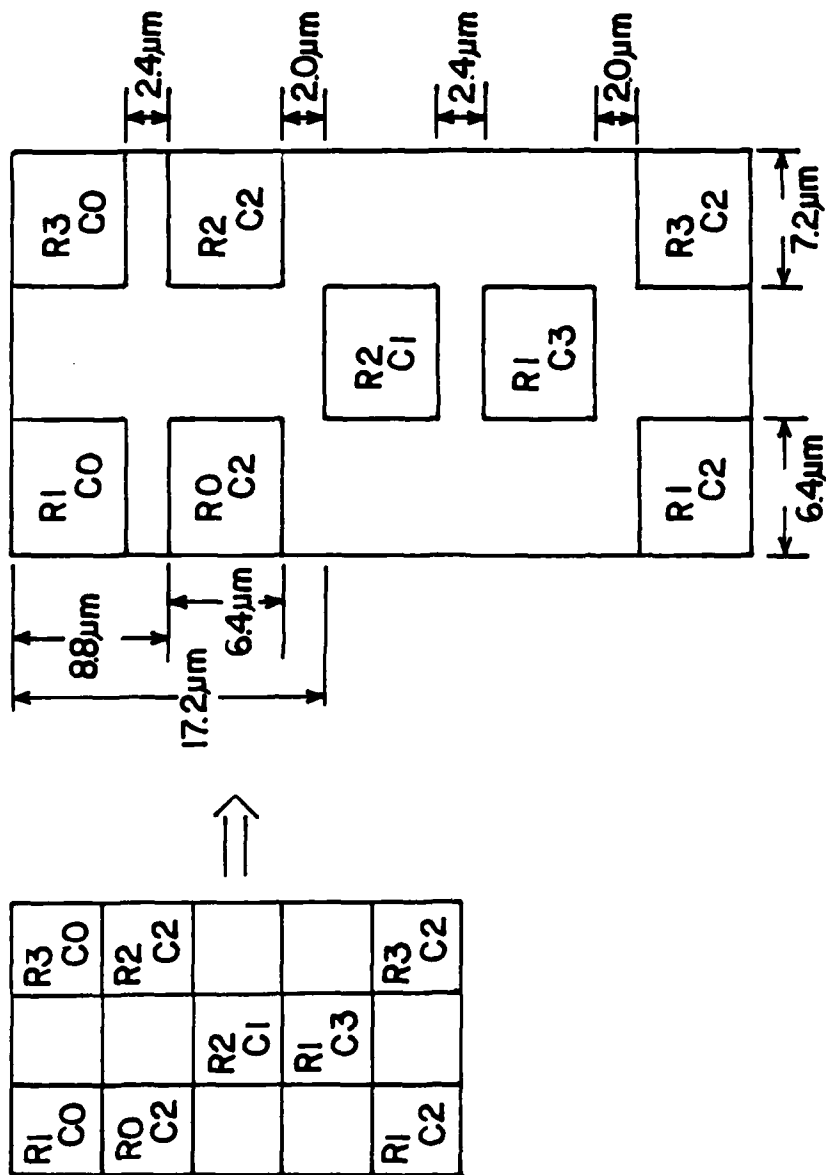


Figure 8. OpticRAM Interleaved Pattern

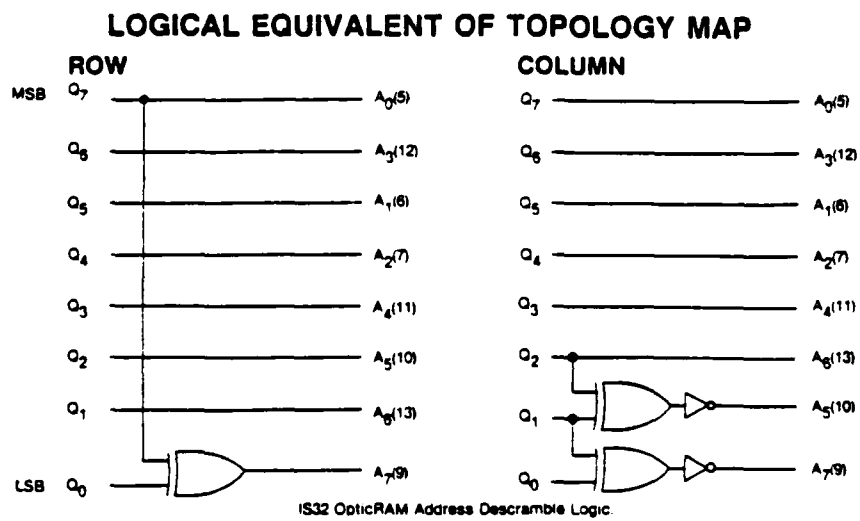


Figure 9. Mapping Circuit Logic

IS32A OPTICRAM TOPOLOGY

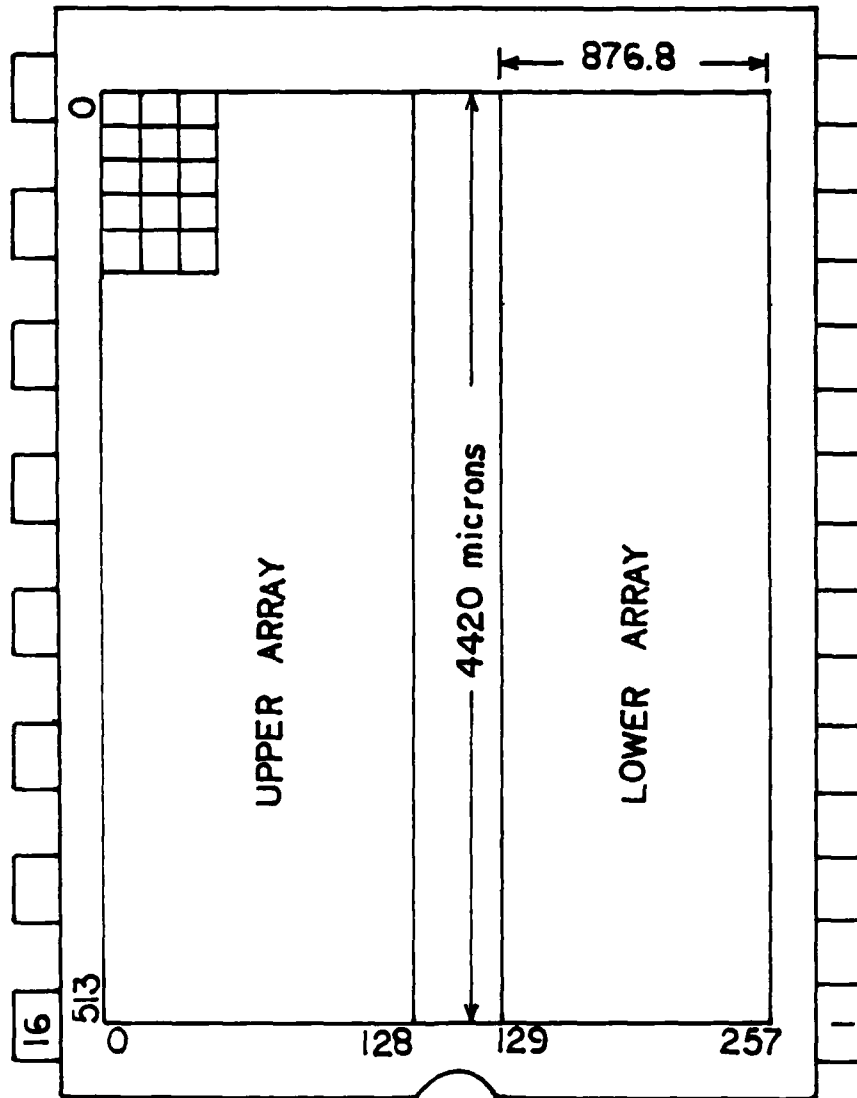


Figure 1C. Cell Placement Grid

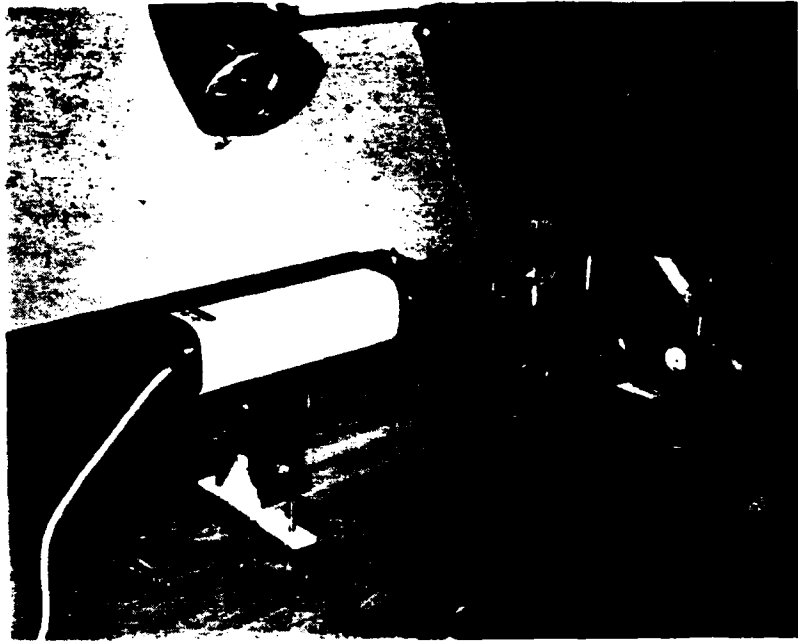


Figure 11. MicronEye Experimental Set-up



Figure 12. MicronEye Experimental Set-up with Computer

photoconductive cell. The MicronEye is interfaced with an Apple Plus II microcomputer and compatible software. This method of operation involves positioning the diffraction pattern, caused by the fiber obstructing the parallel light from the Helium-Neon laser, onto the surface of the OpticRAM. Since the physical size of the OpticRAM chip is so small the positioning is accomplished using a three dimensional (X-Y-Z) positioning table to bring the chip face in the path of the diffraction pattern. Once the pattern is positioned on the OpticRAM, the image is manipulated using the software options. The objective is to bring each band of light together to the point of touching each other by changing the exposure time option in the software. Increasing the exposure time effectively converges the light from each adjacent diffraction band toward the interference node that exists somewhere between the two. Once the two light band images are resolved down to a single pixel, they are effectively as close together as they can be and still be distinguishable. After manipulation the image is stored and then printed out on the graphics printer. Since the printed copy of the diffraction pattern has a resolution no more accurate than one pixel of the entire length, the pattern is physically measured by counting the number of pixels that correspond to the length of the the diffraction image between the nodes. In some instances where it is not possible to resolve the diffraction pattern down to a single pixel, a method of increased accuracy is possible by extending the curvature of each adjacent diffraction band and then by interpolation estimating the point of intersection between the two. With this information similarly as in method A and using equation (2), the diameter of the fiber can be calculated.

IV. INTEGRATED FIBER DIAMETER AND STRENGTH TEST

The two methods for measuring the diameter of a fiber sample were described in Section III. Calculating the diameter of a fiber as previously pointed out is essential in determining the cross sectional area as one part needed in the study of fiber strength. The other however is the tensile test whereby a sample is fractured under a load condition in order to determine the stress applied.

A. SYSTEM DESCRIPTION

The intergrated system of Figure 13 was designed for this purpose in mind. With this system a sample fiber may be measured for size and tensile tested for strength all in one set-up to minimize handling of the fiber. Of course, when working with the accuracies expected in measurements such as these, a high degree of precision is required. Both precision in movement and the desire to minimize handling of the sample were reasons that influenced the design of the integrated system which is described below.

B. DESIGN

The integrated system consists of optical guidance tracks chosen so as to provide smooth precise movement of the laser, photoconductive cells, and the fiber sample in proper positions. The photoconductive cells and strength test frame containing the fiber sample are also capable of additional fine adjustment by means of micrometer positioning tables that are mounted on

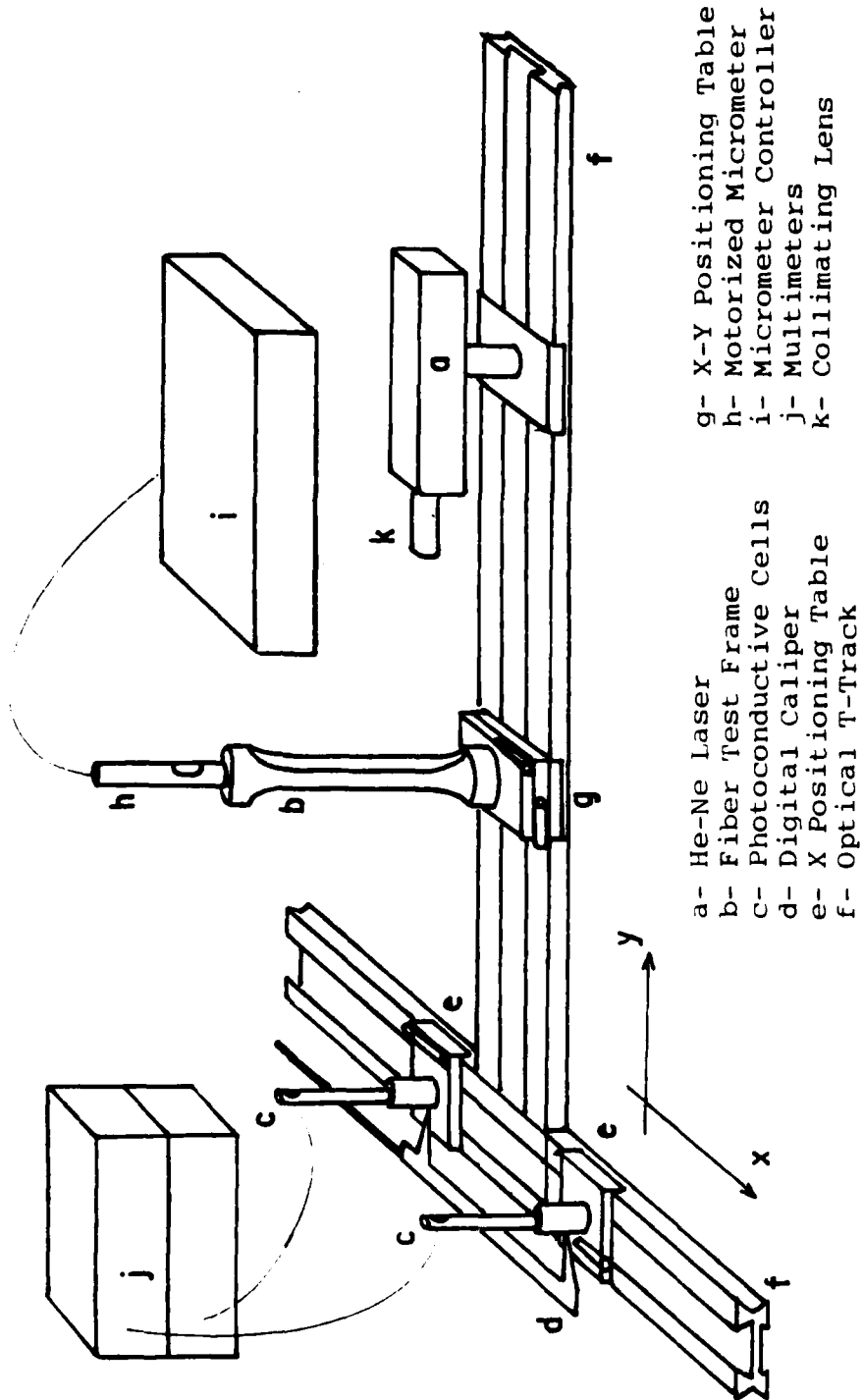
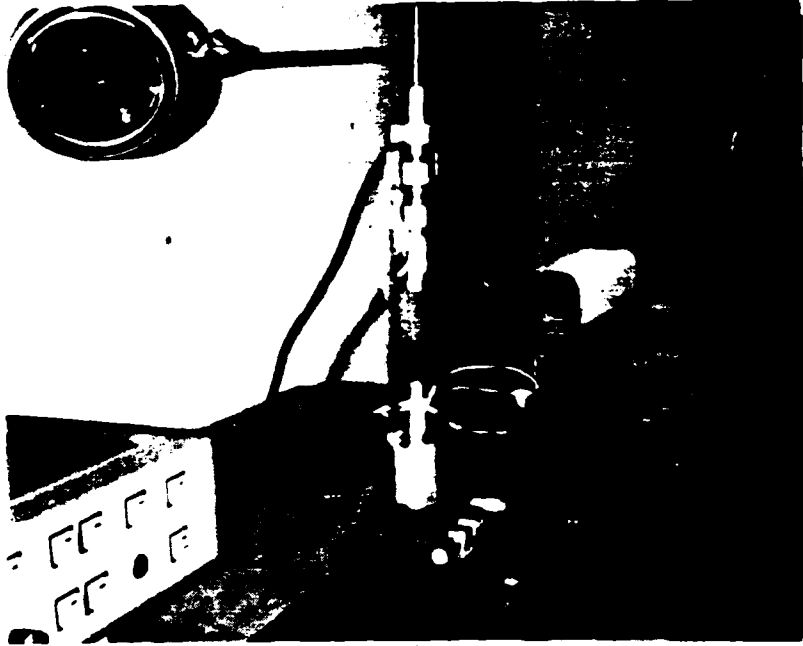


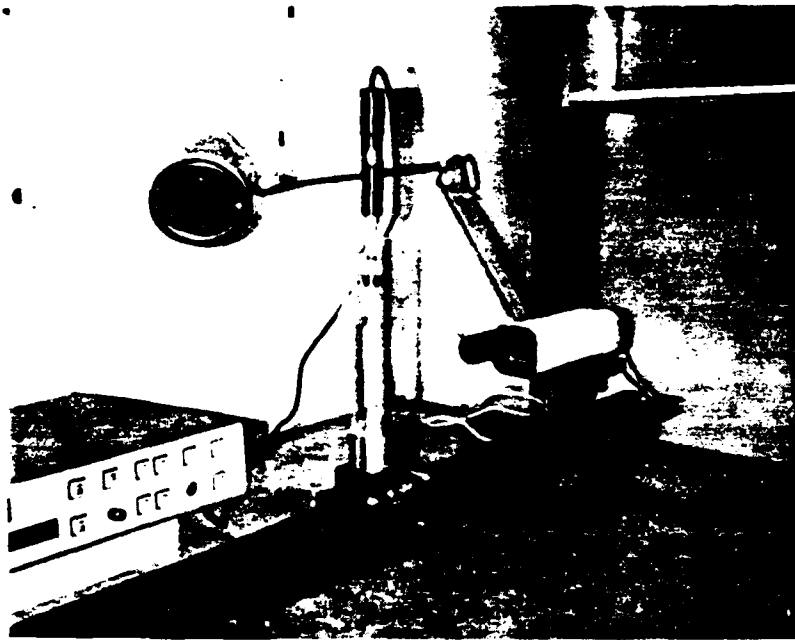
Figure 13. Integrated System Schematic

the coarse positioned track carriers. The photoconductive cells are able to be positioned along the top of the T-track assembly perpendicular to the bottom track by moving the bench carriers and then fine movement on the micrometer driven X-direction positioning table. The longer bottom section of the T-track assembly allows the laser and sample test frame to be positioned anywhere along its length. This makes it possible to determine the best relative location of the laser and sample fiber to the plane of the diffraction pattern to ensure the sharpest image at the photoconductive cells. In addition, the sample test frame is capable of fine adjustment positioning in the X and Y directions to provide precise alignment of the fiber sample in the path of the laser light. A vital part to this entire system is the sample test frame, since this part serves to not only hold the fiber sample for the laser light measurement, but also as a structure for the tensile fracture of the sample. The design of the test frame allows sample gage lengths of zero to 5.0 centimeters to be tested. Spacers in the frame holder enable fiber diameter measurements to be made at three different locations along the fiber length. The entire frame is additionally capable of rotating in its holder, thus exposing different aspects of a sample fiber to the laser light (see Figure 14). Collectively a sample fiber can be examined at different aspect angles from 0-90 degrees, at three separate positions along its length, and for several gage length samples.

The fiber sample itself is held in place by upper and lower V-Jaw mounting fingers. The upper mounting finger is affixed to a load cell with an adapter and the load cell in turn is affixed to the drive head of a motorized micrometer. The motorized micrometer provides the tensile



(a)



displacement and the precise measurement of strain applied to the rigidly mounted fiber sample. The load cell, capable of sensing in the range of 0-150 grams, is used to measure the applied load enabling the determination of the strength of the fiber. Figures 15 through 20 show various experimental set-ups possible with the Integrated System design.

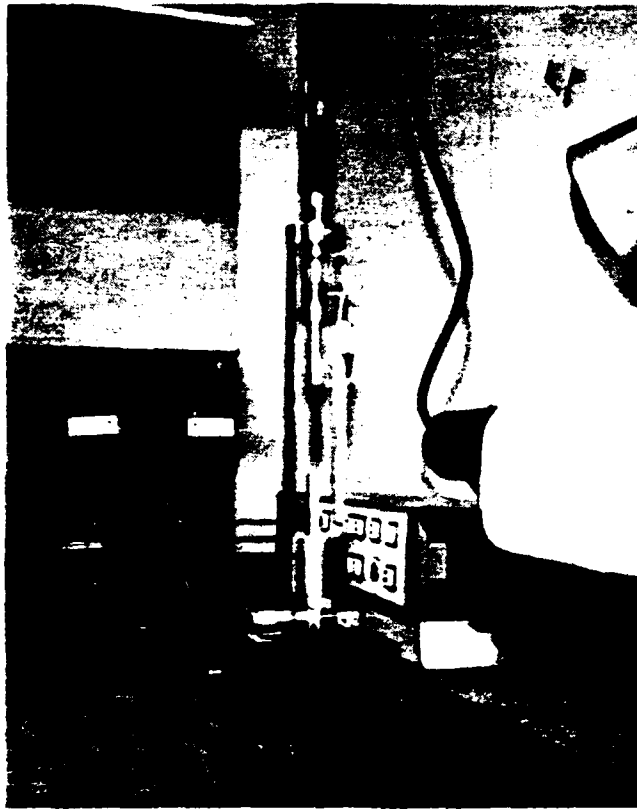


Figure 10. Integrated System



Figure 16. Integrated System

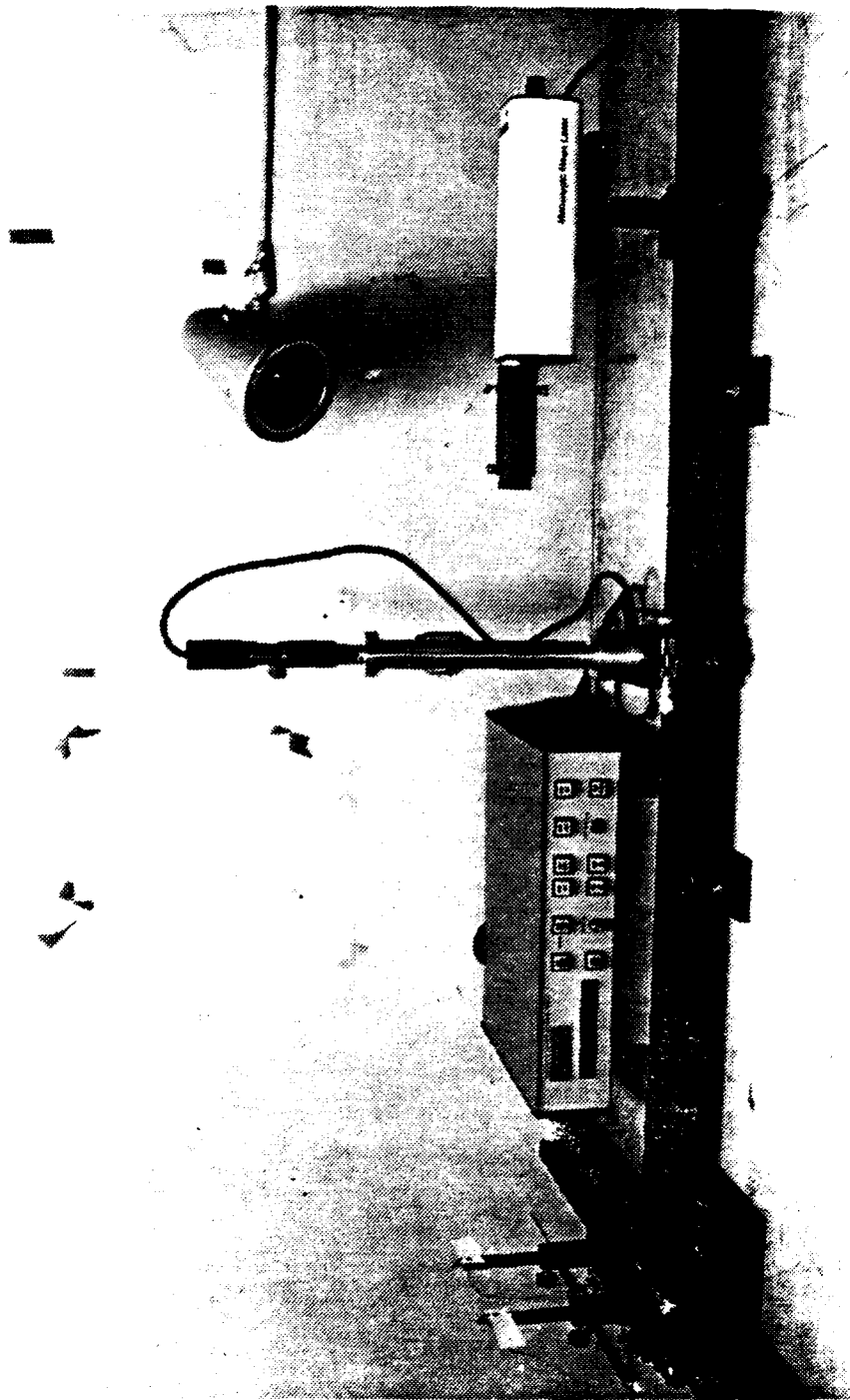


Figure 17. Integrated System

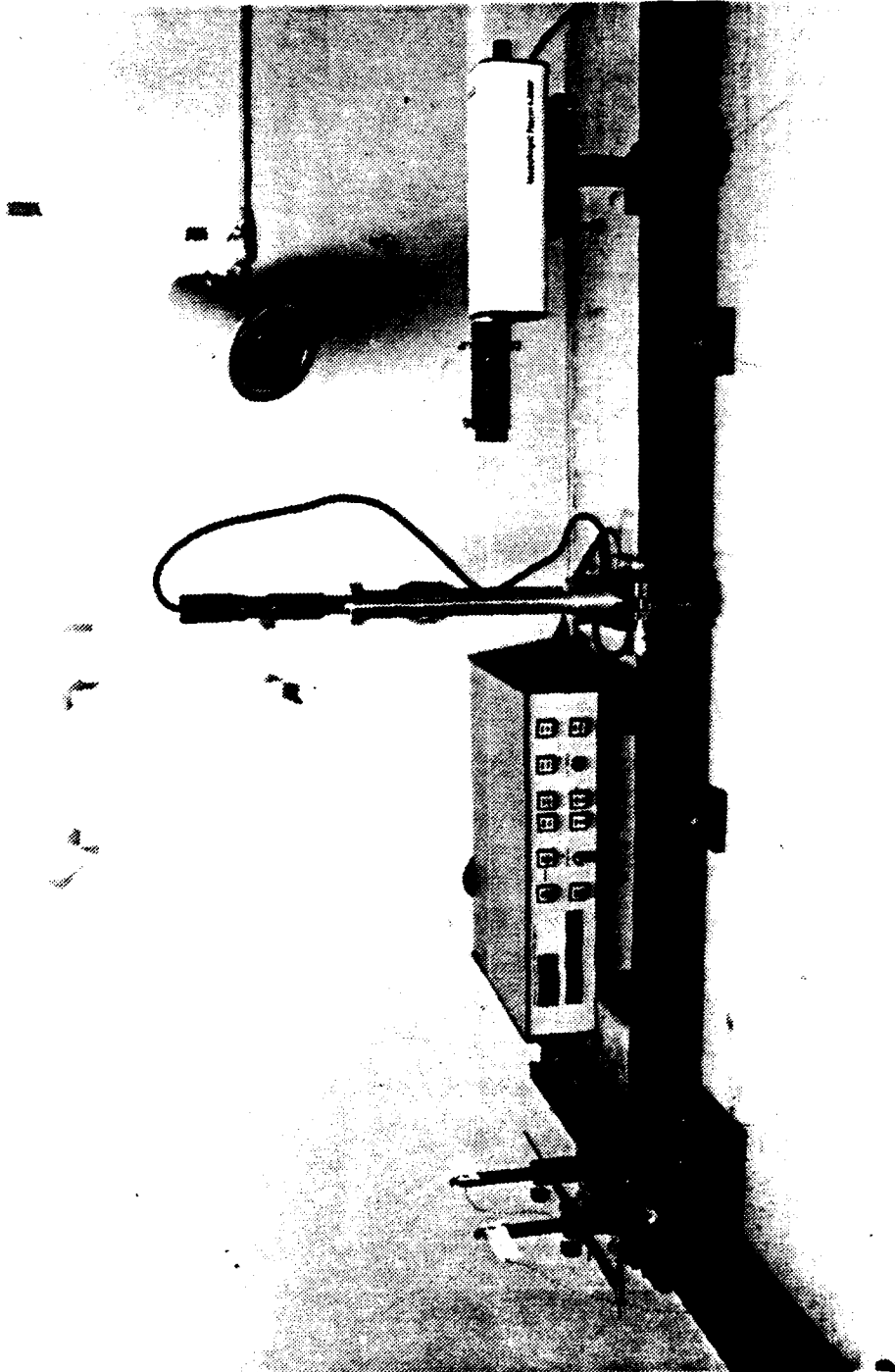


Figure 18. Integrated System
(with Laser Beam)

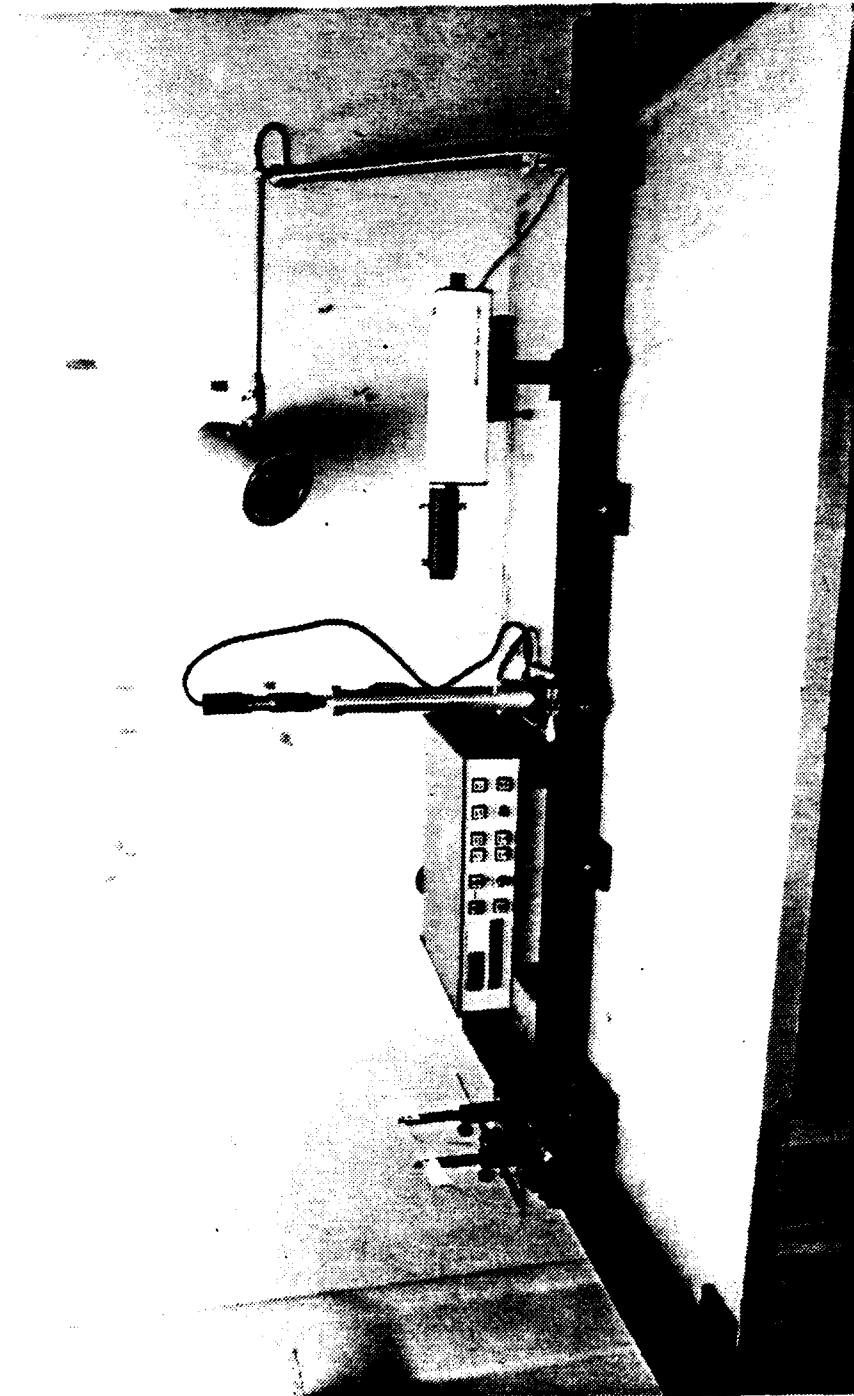


Figure 19. Integrated System

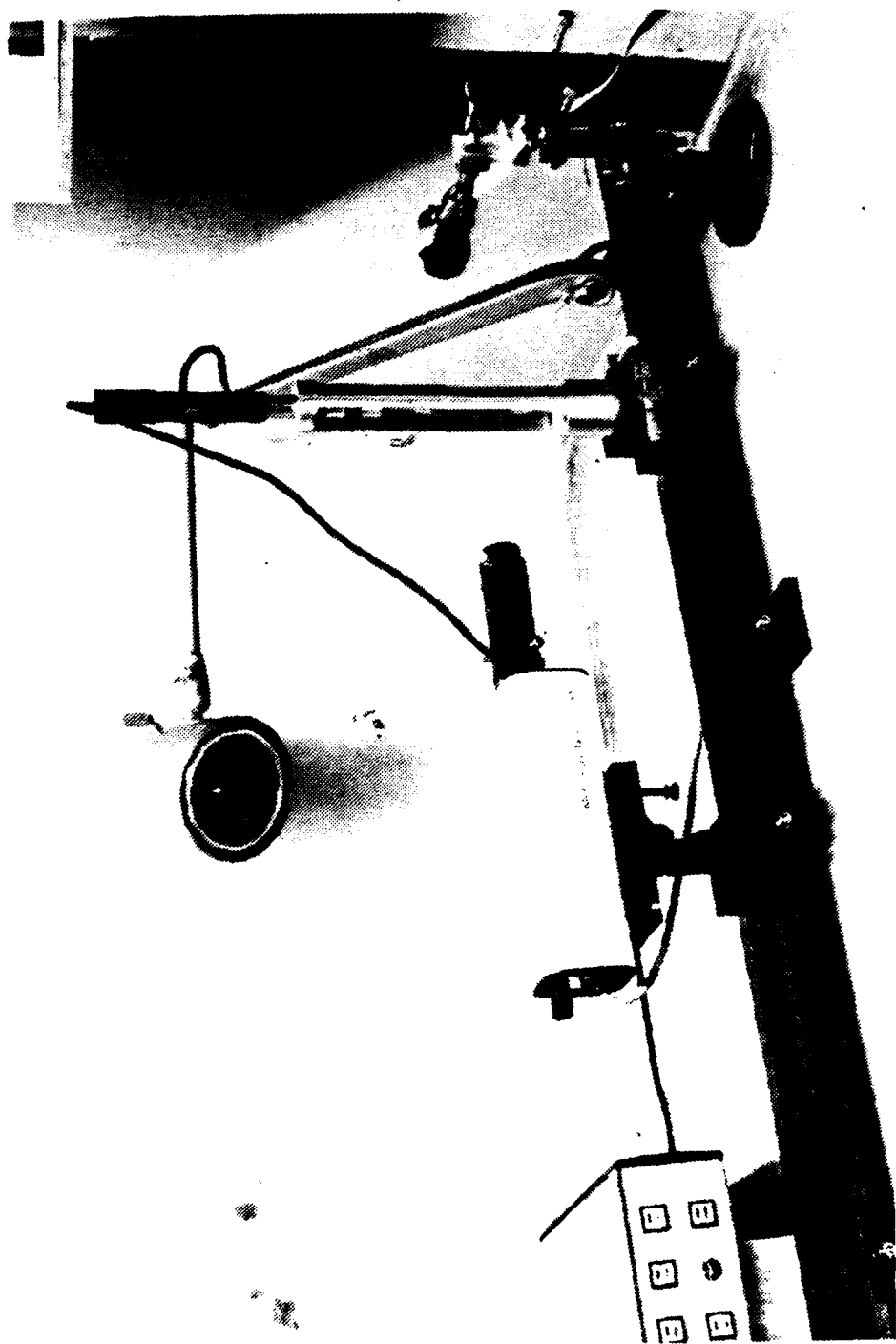


Figure 20. Integrated System

V. DATA COLLECTION

The collection of data was performed using the two methods described on Section III.

A. PHOTOCONDUCTIVE CELL

Prior to recording data for this particular method the initial distance between the two photoconductive cells must be calibrated. This is accomplished by mounting the digital caliper such that the caliper fingers can be adjusted to pass over the light sensitive apertures of the photoconductive cells. Several resistance readings are recorded on the multimeter which correspond to partially or totally covered aperture. This procedure allows the centerline of the aperture to be found by interpolation leading to the correct distance between the two cells. Knowing the calibrated distance, each data measurement involves only obtaining the difference in distance between the photoconductive cell spacing and adding this to the known calibrated distance to find the actual distance for each succeeding measurement.

1. Procedure

The fiber sample used for the collection of data by both methods described in Section III was a Tungsten fiber with an approximate known diameter of 25 microns and with a gage length of 5 centimeters. For the data taken in this study the laser light was focussed on the mid-gage length point or center of the fiber so that all measurements were taken under the

same conditions. Figures 4,11,&12 show the mounted Tungsten fiber used in this experiment.

In this case to begin with, the fiber sample was positioned at a distance L from the plane of the photoconductive cells. L is optimized to provide as sharp of a diffraction band at the plane of the photoconductive cells as possible. The fiber sample was oriented such that measurements were recorded at aspect angles to the laser of straight on (0 degrees) and broadside (90 degrees). A total of 50 measurements for each aspect was performed. Since the distance L provided a wide diffraction band, the second interference node corresponding to $n=2$ provided the best reference for the measurements. The first node appeared too close to the center light spot of the diffraction band caused by the bending of light around the fiber sample. The first nodes were also too close to each other to allow positioning of the photoconductive cells within the minimum constraints of the set-up without changing the distance L . The third node appeared to be too dim for precise positioning. Each measurement consisted of fine positioning the photoconductive cell in the region of the diffraction node until the multimeter indicated the highest resistance reading. Each succeeding measurement involved moving each photoconductive cell away from the node and then repositioning them again thereby starting in a position that required, again finding the node.

2. Data

The raw data obtained from the above procedure is δC . This is shown in Tables I and II. To be useful δC is added to the calibrated distance C in order to find the actual distance X . The distance X is then applied to

TABLE I: MEASUREMENT DATA AND CALCULATED FIBER DIAMETERS FOR METHOD A AT 0 DEGREES

TRIAL	$\delta C(\text{mm})$	$a(\mu)$	TRIAL	$\delta C(\text{mm})$	$a(\mu)$
1	11.90	26.14	26	11.45	26.28
2	11.84	26.16	27	11.45	26.28
3	11.83	26.16	28	11.41	26.29
4	11.81	26.17	29	11.35	26.30
5	11.78	26.18	30	11.31	26.32
6	11.78	26.18	31	11.28	26.33
7	11.69	26.20	32	11.25	26.33
8	11.69	26.20	33	11.19	26.35
9	11.70	26.20	34	11.19	26.35
10	11.70	26.20	35	11.18	26.36
11	11.70	26.20	36	11.17	26.36
12	11.72	26.20	37	11.14	26.37
13	11.68	26.21	38	11.12	26.37
14	11.64	26.22	39	11.09	26.38
15	11.61	26.23	40	11.06	26.39
16	11.58	26.24	41	11.04	26.40
17	11.57	26.24	42	11.03	26.40
18	11.56	26.24	43	11.02	26.40
19	11.48	26.27	44	11.02	26.40
20	11.46	26.27	45	11.02	26.40
21	11.46	26.27	46	10.91	26.44
22	11.43	26.28	47	10.89	26.44
23	11.44	26.28	48	10.85	26.45
24	11.45	26.28	49	10.84	26.46
25	11.45	26.28	50	10.84	26.46

TABLE II: MEASUREMENT DATA AND CALCULATED FIBER DIAMETERS FOR METHOD A AT 90 DEGREES

TRIAL	$\delta C(\text{mm})$	$a(\mu)$	TRIAL	$\delta C(\text{mm})$	$a(\mu)$
1	12.63	25.93	26	12.17	26.06
2	12.62	25.93	27	12.14	26.07
3	12.62	25.93	28	12.07	26.10
4	12.59	25.94	29	12.07	26.10
5	12.56	25.95	30	12.06	26.10
6	12.56	25.95	31	12.06	26.10
7	12.54	25.96	32	12.03	26.10
8	12.54	25.96	33	12.03	26.10
9	12.54	25.96	34	12.03	26.10
10	12.53	25.96	35	12.02	26.11
11	12.52	25.96	36	12.02	26.11
12	12.51	25.96	37	11.97	26.12
13	12.49	25.97	38	11.97	26.12
14	12.48	25.97	39	11.96	26.12
15	12.47	25.98	40	11.96	26.12
16	12.47	25.98	41	11.91	26.14
17	12.46	25.98	42	11.89	26.15
18	12.46	25.98	43	11.85	26.16
19	12.42	26.00	44	11.84	26.16
20	12.39	26.00	45	11.84	26.16
21	12.39	26.00	46	11.82	26.16
22	12.35	26.01	47	11.80	26.17
23	12.34	26.01	48	11.62	26.22
24	12.23	26.05	49	11.54	26.25
25	12.19	26.06	50	11.51	26.26

equation (3), whereby the diameter for that particular measurement is calculated. Calculated values for the diameter of the fiber also appear in Tables I and II.

$$X = C + \delta C \quad (3)$$

$$a = n \lambda L k / X \quad (4)$$

The values for the fiber diameter are rounded off to four significant figures consistent with the uncertainty calculations in the Error Analysis of Appendix B.

B. MICRONEYE

This method, although based on the same principle as that used for the Photoconductive Cell is more sensitive to changes and resolution in the distance L. This is because the distance L as well as the distance between the interference nodes is much smaller and therefore any slight change has a major consequence in follow on calculations. The distance L in this method was adjusted to allow as much of one diffraction band as possible to be exposed on the MicronEye chip. This increases the resolution for the image by having the band occupy as much of the 256 horizontal pixels as possible.

1. Procedure

The procedure for this method is based on the same principles as Method A, however in this method the distance measured is that which corresponds to the horizontal space occupied by the pixels on the OpticRAM IS32A. As discussed in Section III-B, increasing the exposure time has the effect of converging the diffraction bands toward the interference node that

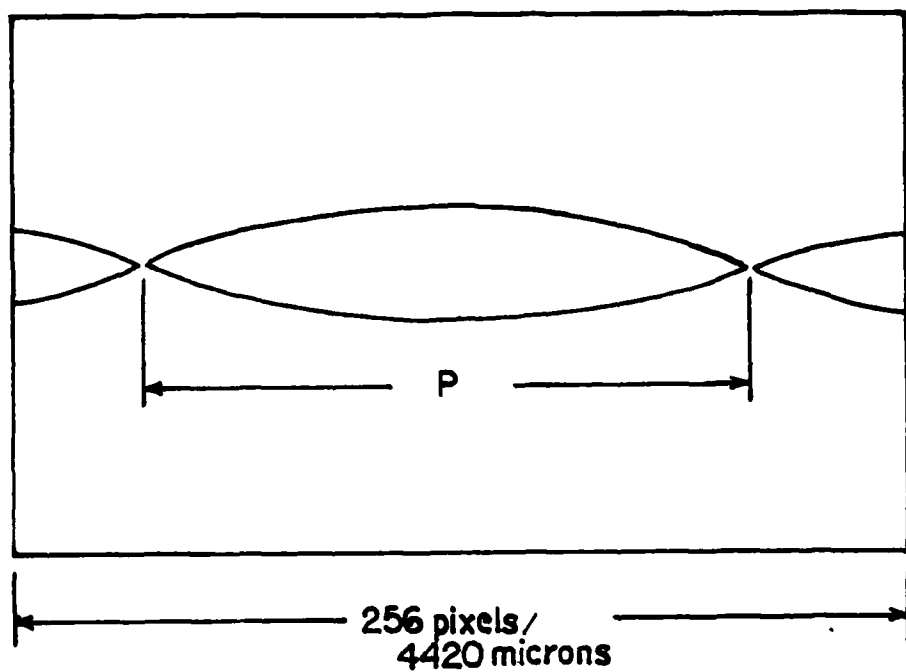
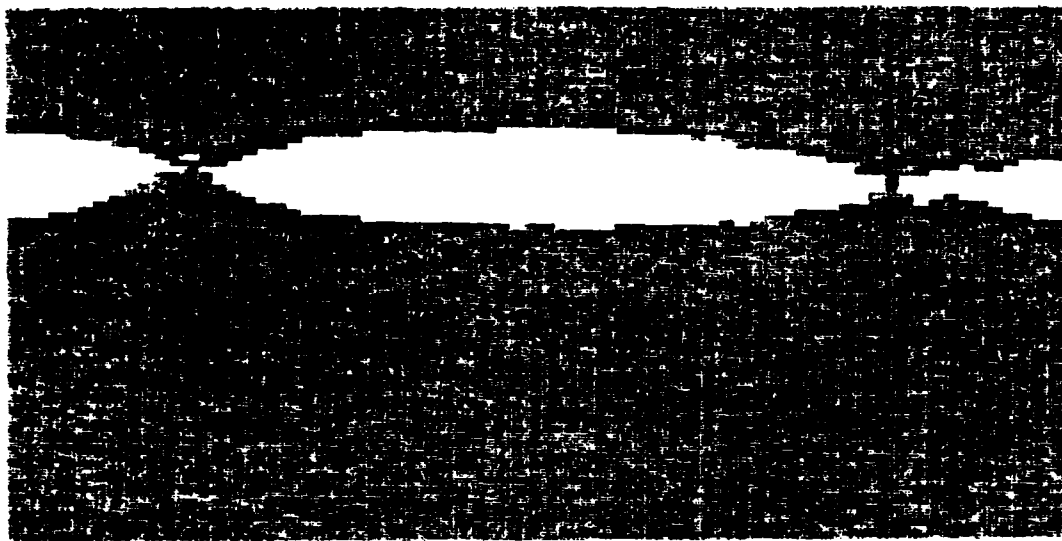
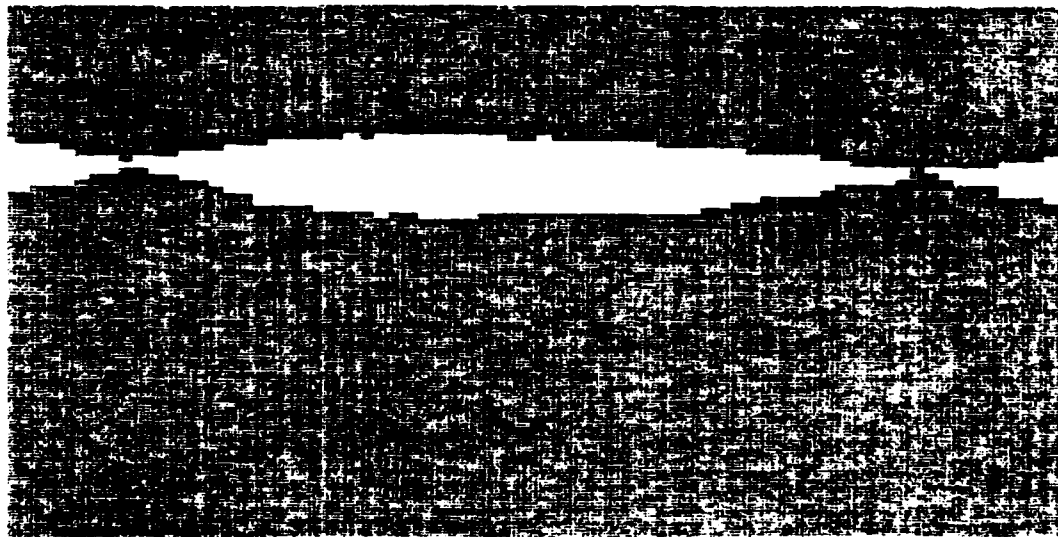


Figure 21. MicronEye Diffraction Band Distance



(a)



(b)

Figure 22. MicronEye Graphics Output Pattern

exists between them. Measuring the length of one adjacent diffraction band is equivalent to the distance d calculated for Method A with the exception that $n=1$ in this case.

2. Data

As seen in Figure 21 , the actual distance of one diffraction band from node to node can be found if the number of pixels the image occupies is known. From equation (5), the number of pixels occupied by a diffraction band is P . Counting P from a typical graphics output as in Figure 22, the distance F in microns can be determined from equation (6).

$$F = P (4420/256) \quad (5)$$

$$a = \lambda L k / F \quad (6)$$

Likewise knowing a value for F in microns, the diameter of the sample can be calculated from equation (6), where k is a conversion constant. Data similar to that collected in Section III-A is shown in Table III. For this particular method 25 measurements were collected each from 0 and 90 degree aspect angles as in Section III-A. Calculated fiber diameters from equation (6) also appear in Table III. Data appears rounded off to four significant figures again consistent with the uncertainty calculations of the Error Analysis in Appendix B.

TABLE III: MEASUREMENT DATA AND CALCULATED FIBER DIAMETERS FOR METHOD B AT 0 AND 90 DEGREES

TRIAL (0 deg)	P(pix)	a(μ)	TRIAL (90 deg)	P(pix)	a(μ)
1	200	25.10	1	202	24.85
2	199	25.23	2	201	24.98
3	198	25.36	3	201	24.98
4	198	25.36	4	200	25.10
5	198	25.36	5	200	25.10
6	198	25.36	6	199	25.23
7	197	25.48	7	199	25.23
8	197	25.48	8	199	25.23
9	196	25.61	9	198	25.36
10	196	25.61	10	198	25.36
11	196	25.60	11	198	25.36
12	194	25.88	12	198	25.36
13	194	25.88	13	198	25.36
14	194	25.88	14	198	25.36
15	193	26.01	15	198	25.36
16	193	26.01	16	198	25.36
17	192	26.15	17	198	25.36
18	192	26.15	18	198	25.36
19	192	26.15	19	197	25.48
20	192	26.15	20	196	25.61
21	191	26.29	21	196	25.61
22	190	26.42	22	196	25.61
23	190	26.42	23	196	25.61
24	190	26.42	24	196	25.61
25	188	26.70	25	195	25.75

VI. STATISTICAL ANALYSIS

Using the data collected and described in Section V with appropriate equations, the diameter of one sample fiber is calculated for each of the two methods previously discussed. To properly analyze this data it is necessary to perform statistical computations in order to present the data in such a way that valid assumptions and comparisons can be made.

To start with, it is of primary interest to obtain the best value of the fiber diameter with the data that is on hand. Since the true value of the fiber is not known, the arithmetic mean or average value is regarded as the best obtainable from the observed data assuming that all observations are made with the same care and under the same conditions as they were in this case.[Ref.11] In this way the mean can be assumed as the best value of a series of measurements in place of the unknown true value. The error of each measurement is the difference between the measured value and the true value. In this case the true value is assumed to be the mean and this error is called the variation. The least squares principle says that for any set of measurements a set of small errors is more probable than a set of large errors and that the set with the highest probability gives the most probable value of a quantity measured [Ref.12]. Therefore the average is more likely to be closer to the actual value if the error or variation in each measurement is as small as possible. The standard deviation of a sample gives a description of the spread and the distribution of the values in the sample. It is descriptive of where individual measurements fall within the

entire sample and is commonly referred to as describing the "normality" of the spread.[Ref. 13] The standard deviation is calculated from the following equation where v is the variation.

$$\sigma_s = (\sum v^2/n-1)^{1/2} \quad (7)$$

$$v = a - \bar{a} \quad (8)$$

Knowing the mean and standard variation a plot of the frequency density of the data can be drawn. This plot, in the form of a histogram, is shown in Figures 23-26 for the fiber diameters of each method and aspect. Based on the shape of the frequency density plot, a bell shaped curve is constructed which is modeled by a normal probability curve. This model was selected because a normal distribution is characteristic of random error measurements such as those presented in Section V. The nicety of a normal distribution is that it gives confidence in the ability to provide further standard statistical treatment[Ref. 14]. A normal distribution gives the luxury of treating a finite number of measurements as if there were an infinite number.

To best describe the mean diameter it is necessary to include standard error. Standard error is seen as indicative of the nearness of the mean to the true value. The ability to quantitize the nearness of the mean to the correct value is the basis for confident use of less than an infinite number of measurements.[Ref. 13] The subject of standard error as it relates to the data of Section V is presented in Appendix B. Table IV gives the mean and standard deviation for each measurement method described in Section III and based on the data presented in Section V.

TABLE IV: MEAN AND STANDARD DEVIATION FOR THE FIBER DIAMETER OF METHODS A AND B

	0 DEG. ASPECT	90 DEG. ASPECT
METHOD A:	$\bar{a} = 26.30\mu$	$\bar{a} = 26.05\mu$
	$\sigma_s = .090\mu$	$\sigma_s = .090\mu$
METHOD B:	$\bar{a} = 25.84\mu$	$\bar{a} = 25.33\mu$
	$\sigma_s = .431\mu$	$\sigma_s = .219\mu$

VI. DISCUSSION OF RESULTS

Results calculated in Table IV clearly show a difference in the mean fiber diameter between the aspects of 0 and 90 degrees for each method of measurement. Likewise there is a difference between the mean diameter for both methods. It was expected that the diameter should be close to the specification value provided by the manufacturer. Both sets of results agree that the fiber diameter is larger when measured from the 0 degree aspect. Figures 23 and 24 show the close agreement of the normal curve comparing both aspects. This is understandable since the standard deviations for each aspect are the same. Not common however are the normal curves of the Microneye method shown in Figures 25 and 26. Each is more spread out than those of Figures 23 and 24 but also understandably so. The number of samples for the Microneye method is half that used in the Photoconductive Cell method. This would normally make a significant difference if the sample size was too small. In this case however, $n = 25$ for the Microneye method is viewed as adequate. The variation for the most part would not change appreciably if a larger sample was used because in this case the variation is inherent in the particular method of measurement. The resolution of each measurement is not as controllable as it is for Photoconductive Cell method. As explained in Section V, the key operation in the Microneye method is to adjust the exposure time of each image to effectively converge the diffraction bands to a single pixel. In some trials this was accomplished but in others it was not and therefore a close approximation was accepted.

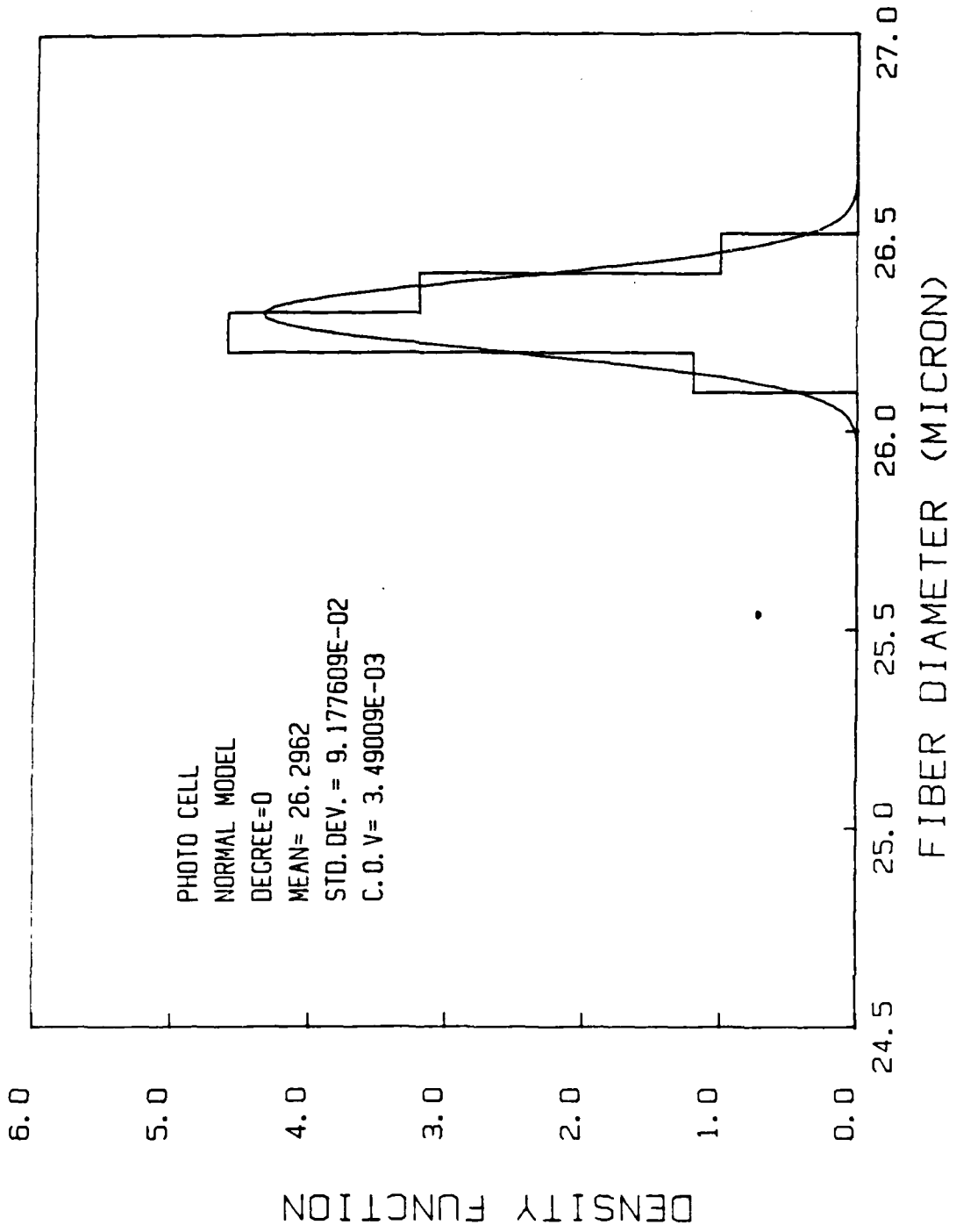


Figure 23. Photocell Method 0 Degree Aspect

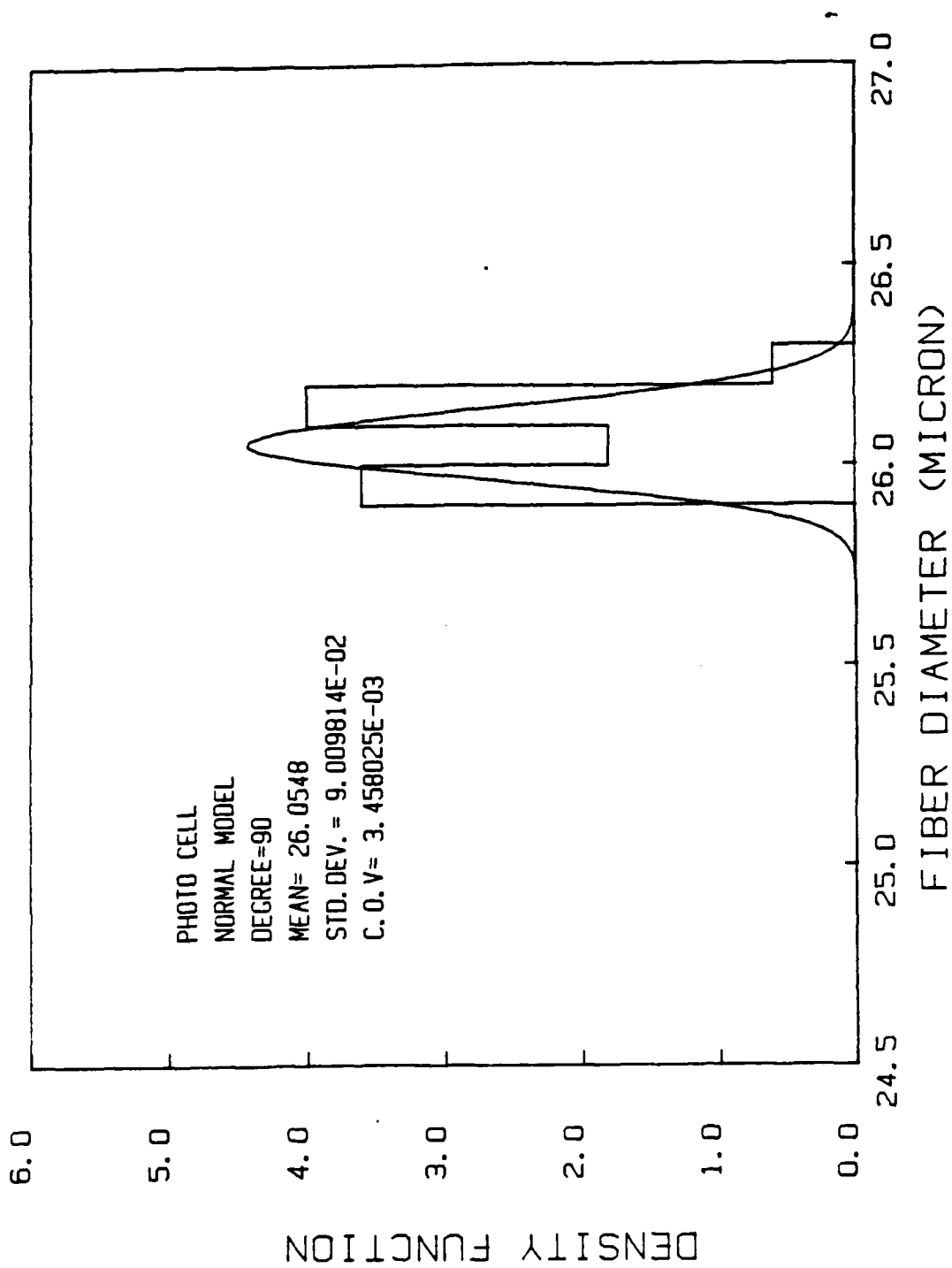


Figure 24. Photocell Method 90 Degree Aspect

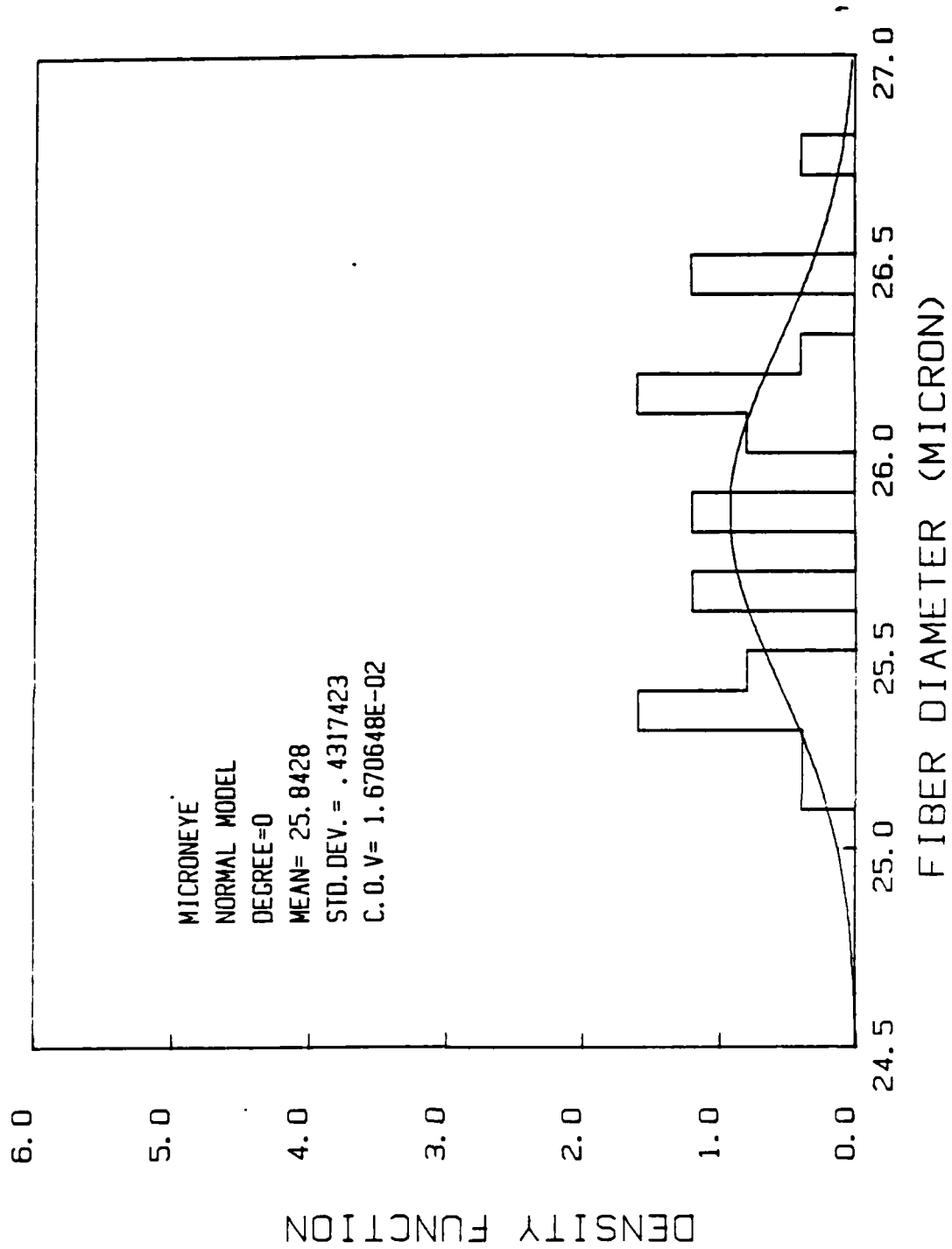


Figure 25. MicronEye Method 0 Degree Aspect

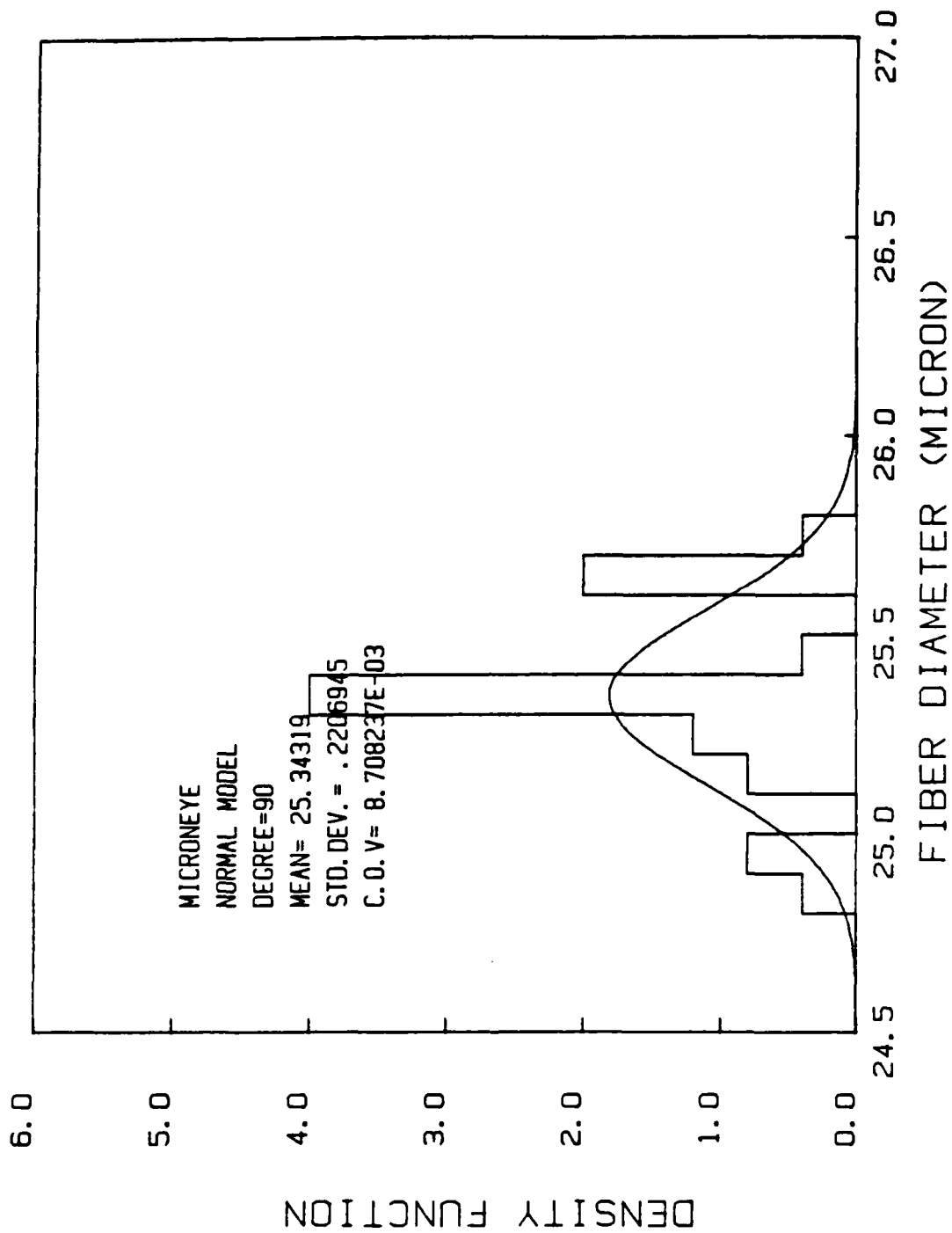


Figure 26. MicronEye Method 90 Degree Aspect

The disparity in the Microneye method is not so much the difference between it and the Photoconductive Cell method, but in the difference between the two aspects of the same method. Figure 25 shows a much more spread out distribution than that of Figure 26. In fact the standard deviation from Figure 25 is nearly double that of Figure 26. From Table IV in Section V there is approximately a 0.5 micron difference between the average diameters of both methods. This may appear significant but is only slightly less than two percent of the average of 26 microns seen here as a better approximation of the true diameter as opposed to the original specification of 25 microns.

To provide a check of accuracy the sample diameter was measured under an optical microscope (X100) with an accuracy of ± 10 microns. The measurement indicated the diameter to be between 20 and 30 microns, not helpful in this case but still a verification that the diameter is in the vicinity expected. As seen by the results of Table IV the methods studied here are much more accurate than that obtained by the optical microscope. This increased resolution clearly favors the use of the diffraction methods as opposed to optical methods.

Though it appears that the data is fairly reliable for the Photoconductive Cell method, in reality there are places for possible error in this method as well. As the distance L , seen in Figure 1 is increased, the small angle approximation approaches the true value of $\text{SIN } \theta$ but at the same time the image projection of the diffraction pattern is more spread out. This has the effect of decreasing the intensity of the diffraction bands and increasing the distance between integer number of nodes. The result is

that the nodes are more difficult to locate due to the sensing limitations of the photoconductive cells. The greater the area of the diffraction band low intensity node the more difficult it is to accurately pinpoint the micrometer adjustment corresponding to the low resistance reading on the multimeter. This in turn results in larger variations in δC . In this particular case the distance L was chosen to hopefully optimize the conditions, but this cannot be quantitatively verified unless several different set-ups are used and the data then compared after final calculations are completed.

Since this study involves a comparison of the two methods of measurement it is necessary to be aware of the possible areas for error and their possible effects. In comparison each method studied has advantages and disadvantages over each other. The Photoconductive Cell method has a higher resolution than the MicronEye method, but has the disadvantage of requiring manual adjustment. The MicronEye method on the other hand is digital and has the potential for automation to improve resolution. Improved resolution is possible by curve smoothing the adjacent diffraction bands to locate the node automatically. This in turn will increase resolution and decrease the amount of human judgement inherent in the Photoconductive Cell method. Both methods do show the variability of the diameter at different aspects of the fiber.

Remarks in the introduction of this study stated that knowing the diameter of a fiber allowed the cross sectional area to be determined using equations of geometry. If the cross section is circular this presents no great task, but as seen from the results this would not be a valid assumption for this particular fiber since the diameter is not uniform. For

this case an elliptical or non-linear approximation would have to be accomplished to obtain a more true approximation of the cross sectional area. This type of approximation is demonstrated in [Ref.15] where an equivalent fiber diameter from an elliptical approximation using the dimensions of the major and minor axis of dumbbell shaped cross section is transformed to a circular cross section. This method used a Scanning Electron Microscope (SEM) to obtain the two dimensional data used in the elliptical approximation. The SEM essentially performs the same type of measurement that is possible with both methods examined in this study. In this case the diameters are determined using the laser light as opposed to SEM cross sectional images. The point emphasized here is that whatever method is used to directly or indirectly calculate the cross section of a fiber, the diameter whether uniform or not has to be determined.

VIII. CONCLUSIONS AND RECOMMENDATIONS

Both methods of fiber diameter measurement demonstrated that the fiber sample was not uniform in diameter. Additionally both methods measure, within two percent of each other, the unknown diameter of the sample fiber. Based on the results it is concluded that the more exact true diameter of the Tungsten fiber sample is 26 microns rather than 25 microns which calculates to approximately four percent larger in diameter than originally assumed.

The methods studied here, when applied to the integrated system discussed in Section IV, should offer an accurate and fairly uncomplicated method of measuring fiber diameters. The integrated system allows less handling of the fiber samples but more flexibility in obtaining data at variable aspects, gage lengths, and sizes less capable when using methods such as SEM and image microscopes. These alternate techniques which normally require extensive preparations are not practical when large sample sizes are desired. The Microneye technique, because of its ability to provide a visual image of a diffraction pattern, is capable of greater improvements to the method used in this study. Because the software provided by Micron Technology Inc., can be altered to provide assorted ways to process the image information obtained, it is suggested that future studies may be conducted to utilize the GREY-16 option of the software. This will require making changes to the assembly language routines of the program. If the program can be altered to provide a curve fit of the approximate shape of a

diffraction pattern, then the node between the adjacent diffraction bands can be resolved with more accuracy and thus provide a better more precise measurement F from equation (5). Additionally to further improve the entire diffraction method, two MicronEye chips could be used to take the place of the photoconductive cells. This would not only have the resolution capability of the photoconductive cell method, but the possibility for automation of the MicronEye method as well. This would allow greater distances to be used decreasing the possibilities of measurement error and further improving the small angle approximation. By incorporating each method together, the diameter measurement could benefit from the advantages of each method separately.

Besides the two methods of measurement adding to the diversity of the integrated system, the tensile strength tester offers a rigid structure for the sample fiber and the entire rail system precise alignment capability seen as very adequate to perform a respectable study of fiber composite reliability.

APPENDIX A. SMALL ANGLE APPROXIMATION

In Section II it was stated that $\text{SIN } \theta$ in the equation $a \text{ SIN } \theta = n\lambda$, could be approximated to equal d/L because the distance L was much larger than the distance d for $\theta \ll 1$. Justification for this assumption is described below for each of the measurement methods described in Section III.

1. Photoconductive Cell: (see Figure 2)

$$a \text{ SIN } \theta = n \lambda \quad (1)$$

where $\theta = \text{TAN}^{-1} d/L \quad (9)$

$$a \text{ SIN } (\text{TAN}^{-1} d/L) = n \lambda \quad (10)$$

using values obtained in Section V for 0 deg. aspect:

$$X = C + \delta C = 77.25\text{mm} + 13.38\text{mm} = 88.63\text{mm}$$

$$d = X/2 = 44.32\text{mm}$$

$$L = 920.75 \text{ mm}$$

then; $d/L = 0.04813$

$$\theta = 2.7557 \text{ radians}$$

$$\text{SIN } \theta = 0.04818$$

The value for $\text{SIN } \theta$ is within .0001 decimal places of d/L . The percentage error 0.1%

2. Microneye: (see Figure 2)

$$a \text{ SIN } \theta = n \lambda \quad (1)$$

where $\theta = \text{TAN}^{-1} F/L \quad (9)$

$$a \text{ SIN } (\text{TAN}^{-1} F/L) = n \lambda \quad (10)$$

using data collected in Section V for 0 deg. aspect:

$$F = 3354.7\mu$$

$$L = 136.98 \times 10^3\mu$$

then; $F/L = 0.024490$

$$\theta = 1.4029 \text{ radians}$$

$$\text{SIN} = 0.024483$$

Again SIN θ is within .0001 decimal places of F/L. The percentage error in this case is 0.04%.

In both cases it is shown that the small angle approximation is justified. An important observation shows that although the relative distances worked with are much smaller in magnitude for the Microneye method, the small angle approximation has a tenth of a percent less error involved than the Photoconductive Cell method which deals with much larger distances.

APPENDIX B. ERROR ANALYSIS

1. Propagation of Errors:

Each of the measured values obtained in Section V are recorded as precisely as possible, however the method of each measurement has a different uncertainty inherent in the measuring system or instrument used. When the data values are used to compute final results, these uncertainties are carried through the calculation procedure as well. To guard against excessive error in the final result it is necessary to know the size of the error after the final calculations such that it can be applied at the end to give the more correct value of the result.[Ref.16] The uncertainty for the calculation of the average fiber diameter for the Photocell method for each aspect angle is shown in the following Table.

TABLE V: DIMENSIONAL DATA FOR METHOD A
AT 0 AND 90 DEGREE ASPECTS

	QUANTITY	VALUE	ERROR
0 deg.	C	77.25 mm	$\pm .01$ mm
	L	36.25 in.	$\pm .06$ in.
	$\delta\bar{C}$	11.38 in.	$\pm .01$ mm
90 deg.	C	77.25 mm	$\pm .01$ mm
	L	36.25 mm	$\pm .06$ in.
	$\delta\bar{C}$	11.38 mm	$\pm .01$ mm

[Ref.16:pp. 72-77] gives equations for the calculations of propagation errors. When quantities are added containing errors their sum has an error equal to the square root of the sums of the squares of the errors.

$$E_s = (E_1^2 + E_2^2 + \dots)^{1/2} \quad (11)$$

The product of two quantities that contain errors has the equation of the form;

$$E_p = \pm AB ((E_a/A)^2 + (E_b/B)^2)^{1/2} \quad (12)$$

The propagation of errors for the quotient is similar to that for the product.

$$E_q = \pm AB ((E_a/A)^2 + (E_b/B)^2)^{1/2} \quad (13)$$

Finally, the conversion of a quantity into other units follows the rule for the product,

$$C (A \pm E_a) = CA \pm CE_a \quad (14)$$

where C is the known constant or conversion factor. Utilizing equations 11 through 14, the propagation error for each method of measurement is carried out. The final results are listed in Table VI.

$$a = n \lambda \cdot L/d \quad (2)$$

$$d = (C + \delta \bar{C})/2 = X/2 \quad (15)$$

$$n = 2$$

$$\lambda = .6328 \mu$$

TABLE VI: UNCERTAINTIES FOR CALCULATIONS OF METHOD A AT 0 AND 90 DEGREE ASPECTS

0 DEGREE ASPECT	90 DEGREE ASPECT
$\bar{d} = 44.32 \pm .01 \text{ mm}$	$\bar{d} = 44.73 \pm .01 \text{ mm}$
$L = 920.75 \pm 1.52 \text{ mm}$	$L = 920.75 \pm 1.52 \text{ mm}$
$\bar{a} = 26.30 \pm .04\mu$	$\bar{a} = 26.05 \pm .04\mu$

TABLE VII: DIMENSIONAL DATA FOR METHOD B AT 0 AND 90 DEGREE ASPECTS

	QUANTITY	VALUE	ERROR
0 deg	\bar{D}	194.3 pixels	$\pm 1.0 \text{ pixels}$
	L	5.393 in.	$\pm .001 \text{ in.}$
90 deg	\bar{D}	198.2 pixels	$\pm 1.0 \text{ pixels}$
	L	5.393 in.	$\pm .001 \text{ in.}$

Again using equations 11 through 14 and the following equations the propagation errors for Method B are calculated and shown in Table VIII.

$$a = n \lambda L/F \quad (6)$$

$$F = D (4420/256) \quad (5)$$

$$n = 1$$

$$\lambda = .6328\mu$$

TABLE VIII: UNCERTAINTIES FOR CALCULATIONS OF METHOD B AT 0 AND 90 DEGREE ASPECTS

0 DEGREE ASPECT	90 DEGREE ASPECT
$\bar{F} = 3354.7 \pm 17.3\mu$	$\bar{F} = 3422.05 \pm 17.3\mu$
$L = 136.98 \times 10^3 \pm 25.0\mu$	$L = 136.98 \times 10^3 \pm 25.0\mu$
$\bar{a} = 25.84 \pm .13\mu$	$\bar{a} = 25.33 \pm .13\mu$

The results of Table VI and VIII indicate that the average fiber diameter for each measurement method has a range that lies between the calculated error based on the uncertainty of the measuring device when such data is carried through an arithmetic operation. In this case the calculation of the fiber diameter is based on equation (6).

2. Standard Error:

In Section VI it was stated that to describe the mean value of the average fiber diameter the use of standard error must be examined. The standard error is given by the following equation;

$$\sigma_m = \sigma_s / (n)^{1/2} \quad (16)$$

where the standard deviation is divided by the square root of the sample size. From the data in Section V and the standard deviation calculated in Section VI, the standard error for each measurement method is calculated and shown below:

TABLE IX: STANDARD ERROR AND STANDARD DEVIATION OF METHODS A AND B AT 0 AND 90 DEGREE ASPECTS

	0 DEGREE ASPECT	90 DEGREE ASPECT
METHOD A:	$\sigma_s = .090\mu$	$\sigma_s = .090\mu$
	$\sigma_m = .013\mu$	$\sigma_m = .013\mu$
METHOD B:	$\sigma_s = .431\mu$	$\sigma_s = .219\mu$
	$\sigma_m = .068\mu$	$\sigma_m = .044\mu$

Normal probability statistics states that the probability that the mean lies within $\pm \sigma_m$ is 68.3% the population mean, within $\pm 2\sigma_m$ is 95.5%, and $\pm 3\sigma_m$ is 99.7%. Using $\pm \sigma_m$ and the mean diameter with respective propagation errors from the previous calculations, the best value equals the mean plus the standard error. For the methods used in this study,

$$\bar{a} = a + \sigma_m \quad (17)$$

TABLE X: MEAN DIAMETERS WITH PROPAGATION AND STANDARD ERRORS FOR METHODS A AND B AT 0 AND 90 DEGREE ASPECTS

	0 DEGREE ASPECT	90 DEGREE ASPECT
METHOD A:	$\bar{a} = 25.84 \pm .20\mu$	$\bar{a} = 25.33 \pm .17\mu$
METHOD B:	$\bar{a} = 26.30 \pm .06\mu$	$\bar{a} = 26.05 \pm .06\mu$

LIST OF REFERENCES

1. Rosen, B.W., "Tensile Failure of Fibrous Composites," AIAA Journal, v.2, no.11, pp. 1985-1991, November 1964.
2. Wagner, H.D. and Phoenix, S.L., "A Study of Statistical Variability in the Strength of Single Aramid Filaments," Journal of Composite Materials, v.18, pp.312-338, July 1984.
3. Halliday, D. and Resnick, R., Fundamentals of Physics, p.691, John Wiley and Sons, Inc., 1981.
4. Nussbaum, A. Phillips, R.A., Contemporary Optics for Scientists and Engineers, p.215, Prentice-Hall, Inc., 1976
5. Tipler, P.A., Modern Physics, p.178, Worth Publishers, Inc., 1978.
6. Halliday, H. and Resnick, R., Fundamentals of Physics, pp.742-745, John Wiley and Sons Inc., 1981.
7. Eisenkraft, A., Physical Optics Using a Helium-Neon Laser, pp.3-5, Metrologic Instruments Inc., 1980.
8. MicronEye Operator's Manual, pp.1-2, Micron Technology Inc., 1983.
9. MicronEye Operator's Manual, pp.D1-D2, Micron Technology Inc., 1983.
10. MicronEye Operator's Manual, pp.D3-D5, Micron Technology Inc., 1983.
11. Barry, B.A., Errors in Practical Measurement in Science, Engineering, and Technology, p.14, John Wiley and Sons, Inc., 1978.
12. Barry, B.A., Errors in Practical Measurement in Science, Engineering, and Technology, pp.23-24, John Wiley and Sons, Inc., 1978.
13. Barry, B.A., Errors in Practical Measurement in Science, Engineering, and Technology, p.31, John Wiley and Sons, Inc., 1978.
14. Barry, B.A., Errors in Practical Measurement in Science, Engineering, and Technology, p.21, John Wiley and Sons, Inc., 1978.
15. Own, S.H., A Statistical Theory of Interfacial Shear Strength Distribution, and its Applications to Carbon Fiber Reinforced Polymer Composites, Ph.D. Dissertation, Washington State University, 1984.
16. Barry, B.A., Errors in Practical Measurement in Science, Engineering, and Technology, pp.72-77, John Wiley and Sons, Inc., 1978.

BIBLIOGRAPHY

Fowles, G.R., Introduction to Modern Physics, Holt, Rinehart, and Winston, Inc., 1968.

Hall, C.W., Errors in Experimentation, Matrix Publishers, Inc., 1977.

Kennedy, J.B. and Neville, A.M., Basic Statistical Methods for Engineers and Scientists, Thomas Y. Crowell Company, Inc., 1976.

McMahon, P.E., "The Relationship Between High Modulus Fiber and Unidirectional Composite Tensile Strength," SAMPE Quarterly, v.6, no.1, October 1974

Poole, L., McNiff, M., Cook, S., Apple II User's Guide, Osborne/McGraw-Hill, 1981.

Young, H.D., Statistical Treatment of Experimental Data, McGraw-Hill Book Company, Inc., 1962.